AGU PUBLICATIONS

JGR

Journal of Geophysical Research: Planets

RESEARCH ARTICLE
10.1002/2017JE005289

Key Points:
- Carbon contents of graphite-saturated Martian basalts are 20 to 1400 ppm at $\log fO_2$ of IW − 0.4 to IW + 1.5 at mantle conditions
- Carbon species in Martian basalts are dominated by CO_3^{2-}
- New model predicts carbon contents of graphite-saturated mantle melts of the Mercury, Mars, and the Moon

Supporting Information:
- Supporting Information S1
- Table S1

Correspondence to:
Y. Li,
yuan.li@gig.ac.cn

Citation:
Li, Y., R. Dasgupta, and K. Tsuno (2017), Carbon contents in reduced basalts at graphite saturation: Implications for the degassing of Mars, Mercury, and the Moon, *J. Geophys. Res. Planets*, *122*, 1300–1320, doi:10.1002/2017JE005289.

Received 16 FEB 2017
Accepted 25 MAY 2017
Accepted article online 1 JUN 2017
Published online 15 JUN 2017

Carbon contents in reduced basalts at graphite saturation: Implications for the degassing of Mars, Mercury, and the Moon

Yuan Li[1,2], Rajdeep Dasgupta[2], and Kyusei Tsuno[2]

[1]Guangzhou Institute of Geochemistry, Chinese Academy of Sciences, Guangzhou, China, [2]Department of Earth Science, Rice University, Houston, Texas, USA

Abstract Carbon contents in reduced Martian basalts at graphite saturation were experimentally studied at 1400–1550°C, 1–2 GPa, and $\log fO_2$ of IW − 0.4 to IW + 1.5 (IW denotes the Fe-FeO buffer). The results show that carbon solubility in Martian basalts, determined by secondary ion mass spectrometry, is 20 to 1400 ppm, increasing with increasing fO_2. Raman and Fourier transform infrared spectroscopic measurements on the quenched silicate glasses show that the dominant carbon species in Martian basalts is carbonate (CO_3^{2-}). The experimental data generated here were combined with literature data on similar graphite-saturated carbon solubility for mafic-ultramafic compositions to develop an empirical model that can be used to predict carbon content of graphite-saturated reduced basalts at vapor-absent conditions:

$$\text{At IW} + 1.7 \geq \log fO_2 \geq \text{IW} - 1:$$
$$\log(C, \text{ppm}) = -3702(\pm 534)/T - 194(\pm 49)P/T - 0.0034(\pm 0.043)\log X_{H2O} + 0.61(\pm 0.07)\text{NBO}/T + 0.55(\pm 0.02)\Delta\text{IW} + 3.5(\pm 0.3) \quad (R^2 = 0.89)$$
$$\text{At IW} - 5.3 \leq \log fO_2 \leq \text{IW} - 1:$$
$$\log(C, \text{ppm}) = 0.96(\pm 0.19)\log X_{H2O} - 0.25(\pm 0.04)\Delta\text{IW} + 2.83(\pm 0.34) \quad (R^2 = 0.6)$$

in which T is temperature in K, P is pressure in GPa, X_{H2O} is mole fraction of water in basalts, ΔIW is the oxygen fugacity relative to the IW buffer, and NBO/T = 2 total O/T − 4 (T = Si + Ti + Al + Cr + P). This model was applied to predict carbon content in graphite-saturated mantle melts of the Mercury, Mars, and the Moon. The results show that graphite may be consumed during the production and extraction of some Martian basalts, and CO_2 released by volcanism on Mars cannot be an efficient greenhouse gas in the early Mars. The lunar mantle carbon may be one of the main propellant driving the fire-fountain eruption on the Moon; however, the Mercurian mantle carbon may not be an important propellant for the explosive eruption on Mercury.

1. Introduction

Carbon content in mantle-derived mafic partial melts plays an important role in determining the distribution and cycle of carbon in different planetary reservoirs. In planetary atmospheres, CO_2 and/or CH_4 can modulate the surface climate and maintain habitable conditions for the origin of life and the formation of biosphere [*Hirschmann and Withers*, 2008; *Kasting*, 1997; *Sagan and Mullen*, 1972; *Sleep and Zahnle*, 2001]. Carbon can also significantly affect the physical and chemical properties of mantle materials and result in chemical differentiation by promoting partial melting [e.g., *Wyllie and Huang*, 1975; *Eggler*, 1978; *Dasgupta*, 2013; *Dasgupta et al.*, 2013a; *Sifré et al.*, 2014]. Carbon-bearing volatiles could also be important propellants for the explosive volcanic eruptions on the Moon and Mercury [*Kerber et al.*, 2009; *Nicholis and Rutherford*, 2009; *Rothery et al.*, 2014; *Rutherford and Papale*, 2009].

Unlike the Earth's present upper mantle, which has maintained a relatively oxidized state with oxygen fugacity about FMQ ± 2 (FMQ = fayalite-magnetite-quartz oxygen buffer) [e.g., *Frost and McCammon*, 2008], the silicate mantles such as those of Mars, Mercury, and also the Moon have been comparatively reducing since the solidification of their magma oceans [*Malavergne et al.*, 2014; *Malavergne et al.*, 2010; *McCubbin et al.*, 2012; *Nicholis and Rutherford*, 2009; *Wadhwa*, 2008; *Namur et al.*, 2016a]. The available studies show that the oxygen fugacity of these planetary mantles may be as reduced as 2–6 log units below the Fe-FeO (IW) buffer [*McCubbin et al.*, 2012; *Wadhwa*, 2008; *Namur et al.*, 2016a]. The

solubility and speciation of carbon in silicate melt, which are mainly controlled by pressure, temperature, melt composition, and fugacities of H_2O, H_2, and O_2, have been studied extensively at conditions corresponding to the Earth's present mantle and crust [e.g., *Duncan and Dasgupta*, 2014; *Holloway et al.*, 1992; *Mysen et al.*, 2011; *Ni and Keppler*, 2013]. However, both the solubility and speciation of carbon in reduced mafic silicate melt, which are more relevant for the reduced silicate mantles of Mars, Mercury, and the Moon, are poorly constrained and are topics of active investigation and debate [*Armstrong et al.*, 2015; *Chi et al.*, 2014; *Dasgupta et al.*, 2013a; *Kadik et al.*, 2004; *Li et al.*, 2015; *Stanley et al.*, 2011; *Stanley et al.*, 2014; *Wetzel et al.*, 2013; *Yoshioka et al.*, 2015; *Li et al.*, 2016]. At the Earth's present upper mantle conditions, carbon in mafic silicate melts is dissolved mainly as carbonates [*Duncan and Dasgupta*, 2014; *Holloway et al.*, 1992; *Mysen et al.*, 2011; *Ni and Keppler*, 2013]. The decrease of carbonate in silicate with decreasing fO_2 implies that the carbon dissolved in reduced silicate melt may be dominated by reduced carbon species. A variety of reduced carbon species have been detected by Raman and/or Fourier transform infrared (FTIR) spectroscopy in reduced, graphite-saturated basaltic melts, which include CH_4 and other C-H molecules [*Chi et al.*, 2014; *Li et al.*, 2015; *Mysen et al.*, 2011; *Li et al.*, 2016], Si-C [*Kadik et al.*, 2004], iron carbonyls $Fe(CO)_5$ and possibly $Fe(CO)_6^{2-}$ [*Stanley et al.*, 2014; *Wetzel et al.*, 2013], and C≡O [*Armstrong et al.*, 2015; *Yoshioka et al.*, 2015]. However, the results of these studies are largely inconsistent with each other. In addition, previous experiments were performed on some specific silicate melt compositions, and the application of these experimental results to different planetary bodies may involve a large uncertainty. Furthermore, to constrain the carbon flux degassed from the reduced mantles, previous studies usually assume that during reduced mantle melting, graphite is present throughout the melting interval [e.g., *Hirschmann and Withers*, 2008; *Stanley et al.*, 2011]. However, whether or not graphite remains stable depends significantly on the degree of partial melting, the carbon abundance in the reduced mantles, and carbon solubility in the reduced mantle melts.

The not fully constrained carbon species and solubility in reduced silicate melts cause the species and budget of carbon degassed from the reduced silicate mantles to the atmospheres to be somewhat uncertain, and thus the quantitative role of carbon in modulating climate of early planets, such as Mars, and the role of carbon in driving explosive volcanism on the Moon and Mercury remain incompletely constrained. In this study, in order to further constrain the carbon speciation and solubility in reduced planetary mantle melts, we first present new experimental results on carbon solubility and speciation in Martian basalts at relevant *P-T-*fO_2 conditions. Then, combing with recent data sets of carbon solubility in reduced, different mafic melts [*Armstrong et al.*, 2015; *Chi et al.*, 2014; *Dasgupta et al.*, 2013b; *Li et al.*, 2015; *Stanley et al.*, 2014; *Wetzel et al.*, 2013; *Li et al.*, 2016; *Duncan and Dasgupta*, 2017], we develop an empirical model that can be used to predict carbon solubility in mantle melts of Mars, Mercury, and the Moon.

2. Methods

2.1. Starting Materials

Starting materials included about 60–70 wt % of a synthetic Martian basalt and about 30–40 wt % mixture of Fe-Ni powder. Three different Martian basalts corresponding to olivine-phyric shergottites Yamato 980459, NWA2990, and Fastball were synthesized (Table 1). These compositions were chosen because they are thought to be Martian mantle-derived primary magmas [*Filiberto et al.*, 2010; *Filiberto and Dasgupta*, 2011; *Filiberto and Dasgupta*, 2015]. The composition of mixture of Fe-Ni powder varied from 5 to 75 wt % Fe in order to control the experimental oxygen fugacity in the range of the Martian mantle (IW − 1 to IW + 1 [*Wadhwa*, 2008]) (Table 2). The synthetic Martian basalts were prepared from high-purity oxides and carbonates. To minimize adsorbed water, SiO_2, TiO_2, Al_2O_3, and MgO powder were each fired over night at 1000°C, Fe_2O_3 at 800°C, MnO_2 at 400°C, $CaCO_3$ at 200°C, and Na_2CO_3 and K_2CO_3 at 110°C. After drying, all the oxides and carbonates were first mixed and ground in ethanol in an agate mortar and dried at room temperature overnight. Well-mixed powders were reduced and decarbonated at 1000°C and the oxygen fugacity of FMQ-2 for 24 h using a CO–CO_2 gas mixing furnace. The mixture of Fe-Ni powder was prepared from high-purity Fe and Ni powder, homogenized by grinding under ethanol in an agate mortar, and dried at room temperature. All the dried materials were stored in a desiccator at 100°C for >24 h before loading into graphite capsule for high-pressure experiments.

Table 1. The Major and Minor Element Compositions of Starting Silicate[a]

	Yamoto 980459	NWA2990	Fastball
wt %			
SiO_2	49.6	51.1	49.29
TiO_2	0.4	0.6	0.73
Al_2O_3	6.0	9.2	8.03
FeO	16.8	16.4	17.99
MnO	0.5	0.4	0.5
MgO	20.2	8.1	12.91
CaO	5.8	11.7	6.72
Na_2O	0.5	1.7	2.94
K_2O	0.0	0.2	0.26
P_2O_5	0.2	0.5	0.81
Total	100.0	100.0	100.18
Mg#	68.4	46.9	56.4

[a]Mg# = XMgO/(XMgO + XFeO); *X* = mole fraction.

2.2. High-Pressure Experiments

All the experiments were conducted using an end-loaded piston cylinder device at 1–2 GPa and 1400–1550°C at the experimental petrology laboratory of Rice University, following assembly and calibration as given in *Tsuno and Dasgupta* [2011]. The pressure and temperature conditions chosen were representative of the conditions at which most Martian basalts were generated [e.g., *Musselwhite et al.*, 2006; *Filiberto et al.*, 2010; *Filiberto and Dasgupta*, 2011, 2015]. Graphite capsule was used as a source of carbon and to ensure graphite saturation of silicate melt. Experiments were pressurized first at room temperature and then heated at the rate of 100°C/min. In order to reduce porosity in the graphite capsules and prevent leakage of Fe-Ni alloy melt, experiments were held at 850°C for 1–3 h and then raised to the desired nominal temperature of the experiments. During the run, temperature was monitored and controlled using a type-C ($W_{95}Re_5$-$W_{74}Re_{26}$) thermocouple. *P-T* uncertainties are estimated to be ±0.1 GPa and ±12°C. All experiments were brought down ≤100°C within 10–20 s by switching off the electricity to the heater.

3. Analytical Methods

3.1. Electron Probe Microanalyzer

Quantitative, wavelength dispersive spectroscopic analyses of major and minor element compositions of silicate melt and alloy melt were carried out on a Cameca SX-100 electron microprobe in NASA Johnson Space Center. For the measurement of major elements in silicate glasses, a beam diameter of 20 μm, 15 kV accelerating voltage, and 10 nA beam current for all elements were used both for standardization and sample measurement. Both synthetic and natural standards were used for calibration: oligoclase for Na, orthoclase for K, fayalite for Fe, rutile for Ti, chromite for Cr, metallic Ni for Ni, apatite for P, rhodonite for Mn, and a synthetic basaltic glass for Al, Ca, Si, and Mg. The peak counting time was 20 s except for Na and K, which were measured for 10 s. For analyzing quenched Fe-Ni alloy melt, the samples and standards were uncoated but surrounded with conductive silver paint to avoid charge buildup during electron probe microanalyzer analysis similar to the technique of *Tsuno and Dasgupta* [2015]. The standards used included pure Ni metal for Ni, pure Fe metal for Fe, and an experimentally synthesized, stoichiometric Fe_3C [*Walker et al.*, 2013] for carbon. Analytical condition for alloy melt analysis was 12 kV accelerating voltage, 80 nA beam current, and 20–30 micron beam diameter. Carbon was analyzed using a LPC2 multilayer spectrometer, and counting times were 10 s at peak and 5 s at each background. An anticontaminant device cooled with liquid N_2 was used to minimize carbon blank concentration, and the amount of carbon contamination from the sample surface was estimated to be ~0.4 wt % by analyzing pure Si and Fe metals, according to the protocol of *Dasgupta and Walker* [2008].

3.2. Secondary Ion Mass Spectrometry

The bulk carbon and water contents in the quenched silicate glasses were determined using a Cameca IMS 1280 ion microprobe at Woods Hole Oceanographic Institution, using the same procedures and standardization as described in previous studies [*Chi et al.*, 2014; *Dasgupta et al.*, 2013a; *Li et al.*, 2015, 2016]. The Cs^+ primary beam current was 1 nA, and the beam was rastered over ~30 × 30 μm^2 area. A secondary voltage was 10 kV, with electron gun compensation for positive charge buildup on the sample surface. A secondary field aperture was used to block transmission of ions from outside of the innermost ~10 × 10 μm^2 of the analysis crater, therefore effectively minimizing any potential carbon surface contamination in the measurement. Calibration for H_2O and CO_2 were obtained by replicate measurements of $^{12}C/^{30}Si$ and $^{1}H^{16}O/^{30}Si$ ratios in standard glasses of basaltic composition [*Helo et al.*, 2011]. About 3–6 spots were analyzed for

Journal of Geophysical Research: Planets

10.1002/2017JE005289

Table 2. Summary of Experimental Conditions, Products, and Results[a]

Run No.	Starting Materials	Run Duration (Hours)	Pressure (GPa)	Temperature (°C)	logfO_2 ΔIW[b]	logfO_2 ΔIW[c]	H_2O in SM (SIMS) (wt %)	H_2O in SM (FTIR) (wt %)	C in Metal (wt %)	C in SM (SIMS) (ppm)	C in SM (FTIR) (ppm)	Cal C in SM (ppm)[d]	Cal C in SM (ppm)[e]	NBO/T (SM)[f]	$D^{metal/silicate}$ (Carbon)
G403	Yamato + Fe(5 wt %) − Ni(95 wt %)	24	1.0	1400	0.43	1.24	0.24 ± 0.00	0.14 ± 0.01	4.08 ± 2.13	576 ± 20	1088 ± 222	314	173	1.4	71 ± 37
G404	Yamato + Fe(5 wt %) − Ni(95 wt %)	10	1.5	1500	0.68	1.51	0.51 ± 0.12	0.3 ± 0.01	3.19 ± 2.07	1388 ± 566	2381 ± 678	736	442	1.6	23 ± 18
G405	NWA + Fe(30 wt %) − Ni(70 wt %)	5	2.0	1550	−0.14	0.72	0.55 ± 0.03	0.3 ± 0.01	5.73 ± 1.45	200 ± 67	108 ± 2	125	75	1.3	286 ± 120
G407	NWA + Fe(30 wt %) − Ni(70 wt %)	14	1.5	1450	−0.15	0.68	0.59 ± 0.02	0.26 ± 0.04	4.89 ± 1.05	162 ± 31	86 ± 16	88	49	1.4	302 ± 87
G408	Fastball + Fe(50 wt %) − Ni(50 wt %)	24	1.0	1400	−0.78	−0.05	0.09 ± 0.00	0.05 ± 0.01	3.07 ± 0.52	31 ± 2	<d.l	16	9	1.3	980 ± 179
G409	Fastball + Fe(75 wt %) − Ni(25 wt %)	10	2.0	1500	−1.05	−0.39	0.09 ± 0.00	0.04 ± 0.01	4.68 ± 0.38	21 ± 1	<d.l	8	5	1.3	2267 ± 196

[a]SM = Martian basaltic silicate melt. <d.L. below detection limit. For silicate glasses of each sample, 3–6 spots were analyzed using SIMS and 2–5 spots were analyzed using FTIR.
[b]Ideal fO_2. See section 4.2 for details.
[c]Nonideal fO_2. See section 4.2 for details.
[d]The calculated carbon content at graphite-saturation using the model of *Stanley et al.* [2011].
[e]The calculated carbon content at graphite-saturation using the model of *Holloway et al.* [1992].
[f]NBO/*T* = 2 total O/T − 4 (T = Si + Ti + Al + Cr + P).

each sample glass, and each spot included 10 analytical cycles. During each cycle, a sequence of ^{12}C, $^{1}H^{16}O$, and ^{30}Si was recorded and intensity ratios of $^{12}C/^{30}Si$ and $^{1}H^{16}O/^{30}Si$ were converted to C and H (reported as H_2O) contents. After each 3–5 analytical spots on the sample glass, one or two analyses were performed on the standard glass (ALV 519-4-1) for checking the possible deviation and accuracy during the analysis. Similar to the study of *Li et al.* [2015], during the analytical session, no considerable deviation was observed and the calculated CO_2 content (166 ± 5 ppm) of the standard glass (ALV519-4-1) was in good agreement with its nominal value (165 ppm).

3.3. Raman and FTIR Spectroscopy

Raman and Fourier transformed infrared (FTIR) spectroscopy were used for determining and quantifying the possible C–H–O species in the silicate glasses, following methodologies detailed in recent studies [*Chi et al.*, 2014; *Dasgupta et al.*, 2013a; *Li et al.*, 2015, 2016]. A Renishaw inVia Raman microscope equipped with a 514 nm laser at Rice University was employed. Raman spectra were collected in the frequency range of 200–4500 cm^{-1} with 1 cm^{-1} resolution, using a 50× objective lens and output power of 23 mW. Spectrum at each point in this study was accumulated 2 times with exposure time about 200 s to detect the possible C–H–O species with very low contents.

FTIR spectroscopy with a Thermo Nicolet Fourier Transform Infrared Spectrometer was employed following the protocol in the recent studies [*Duncan and Dasgupta*, 2014, 2015; *Li et al.*, 2015, 2016]. Sample glasses were doubly polished to thicknesses of about 200–300 μm. Spectra were recorded with 4 cm^{-1} resolution, from 650 to 4000 cm^{-1}, averaging 128 scans. A nitrogen purge was used to eliminate atmospheric gasses with backgrounds collected before each analysis.

4. Results

4.1. Texture of the Experimental Products

All the experiments produced quenched blobs of Fe-Ni alloy melt embedded in silicate glasses (Figure 1). The silicate melts in all the runs were quenched into glasses. The alloy melts exsolved into two phases during quench. The bright one is a Ni-rich alloy phase, and the gray one is an Fe-rich phase (Figure 1). Runs G403, G404, and G409 contained about 15–30% silicate minerals (clinopyroxene ± olivine) at the bottom of the sample capsules.

4.2. Major Element Compositions and Estimation of Oxygen Fugacity

The major and minor element compositions measured for coexisting silicate and alloy melts are tabulated in Table 3. Compared to the compositions of starting silicate, the silicate melt compositions were slightly FeO-rich (up to 22 wt %), probably due to oxidation of a small fraction of Fe in the alloy during the run. In Fe-Ni-C alloy melt, the Fe content is between 7.4 and 71.8 wt %, Ni is between 23.4 and 91.1 wt %, and C is between 3.2 and 5.7 wt %.

Following the method used in our previous studies [*Chi et al.*, 2014; *Dasgupta et al.*, 2013a; *Li et al.*, 2015, 2016], the oxygen fugacity (fO_2) prevailing during the experiments was calculated from the coexistence of Fe-rich alloy melt and silicate melt with finite FeO content using the following equilibrium:

$$\mathrm{FeO\ (silicate\ melt)} = \mathrm{Fe\ (alloy\ melt)} + 1/2O_2 \tag{1}$$

from which the fO_2 relative to fO_2 of the iron-wustite buffer (IW), at any given *P-T*, can be defined as

$$\Delta \mathrm{IW} = 2\ \log\left(a_{\mathrm{FeO}}/a_{\mathrm{Fe}}\right) = 2\ \log\left(X_{\mathrm{FeO}}\gamma_{\mathrm{FeO}}/X_{\mathrm{Fe}}\gamma_{\mathrm{Fe}}\right) \tag{2}$$

The a_{FeO} represents the activity of FeO component in silicate melt; a_{Fe} represents the activity of Fe component in alloy melt; X_{FeO} and X_{Fe} are the mole fractions of FeO in silicate melt and Fe in alloy melt, respectively; and γ_{FeO} and γ_{Fe} are the activity coefficients of FeO in silicate melt and Fe in alloy melt, respectively. Calculations of fO_2 using both ideal ($\gamma_{FeO} = 1$ and $\gamma_{Fe} = 1$; ideal fO_2) and nonideal solution models (nonideal fO_2) were performed. The fO_2 calculation using the nonideal solution model was performed assuming $\gamma_{FeO} = \sim 1.5$ [*Holzheid et al.*, 1997; *O'Neill and Eggins*, 2002]. Activity coefficients of Fe in Fe-rich melt, γ_{Fe}, were calculated using the ε approach, which takes into account the nonideal interaction between all the components in the Fe-rich alloy melt [*Ma*, 2001; *Wood et al.*, 2013]. The online "Metal Activity Calculator" (http://

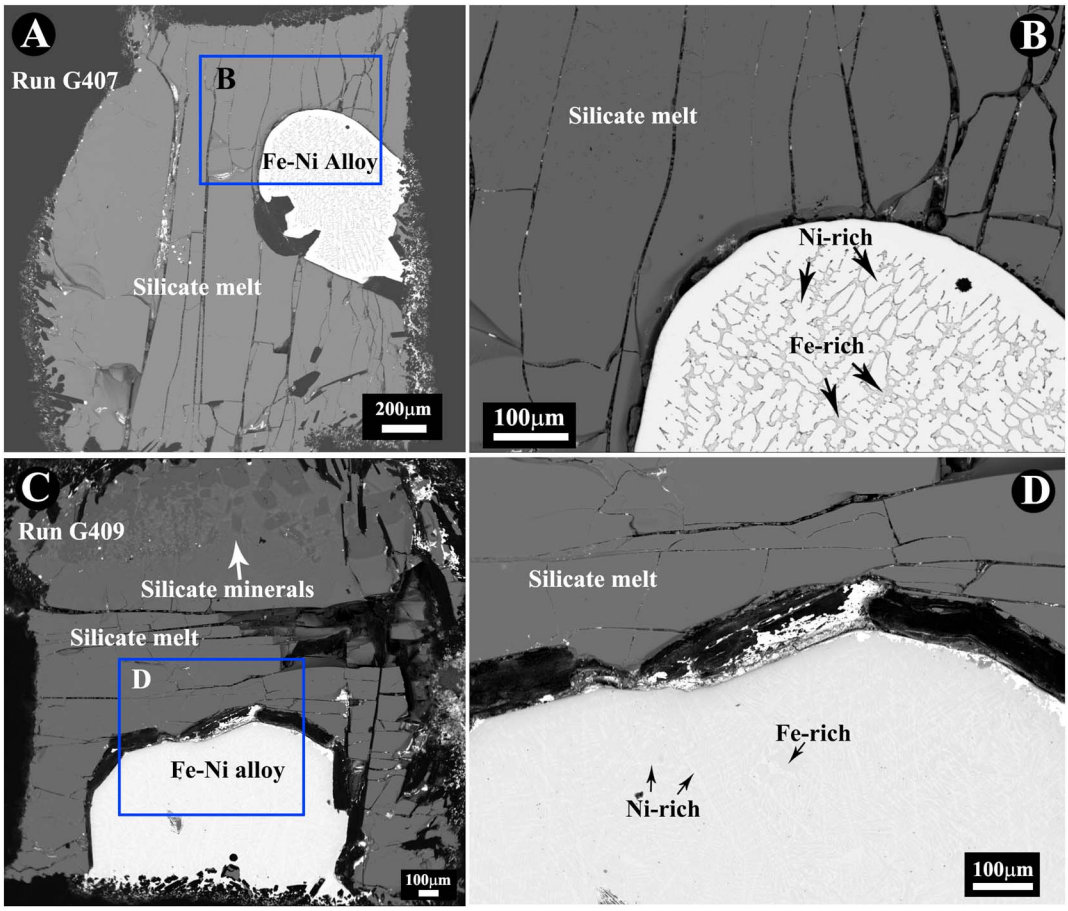

Figure 1. Selected backscattered electron images of run products. (a) Coexistence of quenched silicate melt and Fe-Ni-C alloy melt from run G407. (b) Detailed texture of quenched silicate melt and Fe-Ni-C alloy melt from run G407. (c) Coexistence of quenched silicate melt, Fe-Ni-C alloy melt, and silicate minerals (at the bottom of the sample capsule) from run G409. (d) Detailed texture of quenched silicate melt and Fe-Ni-C alloy melt from run G409. Note that in the alloy, the bright phase is Ni-rich, and the gray phase is Fe-rich.

www.earth.ox.ac.uk/~expet/metalact/) provided by the University of Oxford [*Wood et al.*, 2013] was used to calculate the Fe activity in alloy melt.

The calculated ideal fO_2 values are, in general, ~0.7 log units lower than the nonideal fO_2 values, and the nonideal fO_2 values of all the runs were between IW − 0.39 and IW + 1.51 (see Table 2). The consistent difference between the ideal fO_2 and the nonideal fO_2 and the nearly perfect correlation between the nonideal fO_2 and carbon solubility (see below) indicate that using the ε approach to estimate the activity coefficient of Fe in the Fe-Ni alloy with up to 90 wt % Ni is still valid. All the fO_2 values mentioned hereafter refer to nonideal fO_2 values.

4.3. Bulk Water Content and C–H–O Species in Silicate Melt

The data of bulk water content in silicate melt determined using secondary ion mass spectrometry (SIMS) are tabulated in Table 2. The bulk water content in silicate melts of runs G403–G407 ranges from 0.24 to 0.59 wt %, whereas in silicate melts of runs G408 and G409 it is about 0.09 wt %. All these data are comparable to previous, similar studies on carbon solubility in reduced basaltic melts [*Armstrong et al.*, 2015; *Chi et al.*, 2014; *Stanley et al.*, 2014; *Dasgupta et al.*, 2013a; *Li et al.*, 2015, 2016].

Typical Raman and FTIR spectra are shown in Figure 2. The typical peaks of H_2 (~4100 cm^{-1}) and CH_4 (2900 cm^{-1}) as observed normally for graphite-saturated silicate melts with similar H_2O content and $\log fO_2 < IW - 1$ were not observed from the present Raman spectra (Figure 2a). The asymmetrical

Table 3. Major and Minor Element Compositions of Silicate Melt and Alloy Melt (in wt %)[a]

Run No	SiO_2	TiO_2	Al_2O_3	Cr_2O_3	FeO	MnO	MgO	NiO	CaO	Na_2O	K_2O	P_2O_5	Total	NBO/T	C	Fe	Ni	Total
								Silicate Melt									Alloy Melt	
G403	48.5	0.8	8.4	0.0	16.9	0.6	13.0	0.9	9.9	0.7	0.0	0.2	100.0	1.4	4.1	9.6	88.1	101.8
1σ	0.9	0.1	0.6	0.0	0.6	0.1	1.3	0.3	0.7	0.1	0.0	0.1	1.5		2.1	0.1	1.6	0.9
G404	48.6	0.6	6.8	0.0	18.3	0.6	16.3	1.6	7.7	0.6	0.0	0.2	101.3	1.6	3.2	7.4	91.1	101.7
1σ	0.1	0.0	0.1	0.0	0.2	0.0	0.1	0.1	0.1	0.1	0.0	0.0	0.2		2.1	0.2	1.8	0.5
G405	46.9	0.6	8.7	0.0	20.2	0.5	8.0	0.4	11.8	1.8	0.2	0.4	99.4	1.3	5.7	24.2	71.7	101.7
1σ	0.3	0.0	0.1	0.0	0.2	0.1	0.1	0.0	0.1	0.1	0.0	0.1	0.7		1.4	0.5	1.7	1.1
G407	45.2	0.6	8.7	0.0	20.5	0.4	7.9	0.3	11.7	1.7	0.2	0.4	97.5	1.4	4.9	24.7	71.1	100.8
1σ	0.4	0.0	0.1	0.0	0.2	0.0	0.1	0.1	0.1	0.1	0.0	0.0	0.6		1.1	0.4	1.4	0.8
G408	48.0	0.7	8.1	0.0	20.9	0.5	11.0	0.1	6.6	2.5	0.3	0.4	99.1	1.3	3.1	47.7	49.0	99.7
1σ	0.6	0.0	0.2	0.0	0.2	0.0	0.1	0.0	0.1	0.1	0.0	0.1	0.9		0.5	1.4	1.9	0.4
G409	47.7	0.8	8.6	0.0	21.8	0.5	11.2	0.0	6.6	2.4	0.3	0.4	100.2	1.3	4.7	71.8	23.4	99.8
1σ	1.0	0.0	0.2	0.0	0.2	0.0	0.2	0.0	0.1	0.1	0.0	0.1	1.5		0.4	1.1	1.4	0.3

[a]NBO/T = 2 total O/T − 4 (T = Si + Ti + Al + Cr + P). For each sample, 10–20 spots were analyzed, and 1σ is the standard deviation based on the replicate analyses.

broadband between 3350 and 3650 cm^{-1} are associated with OH^- ions and molecular water. The peak at ~2110 cm^{-1}, which was proposed to be iron carbonyl by *Stanley et al.* [2014] and *Wetzel et al.* [2013] or to be C≡O by *Yoshioka et al.* [2015] and *Armstrong et al.* [2015], is not present in the Raman spectra.

Typical FTIR spectra are shown in Figure 2b. Figure 2b shows that spectra of the silicate glasses synthesized at relatively oxidized conditions (IW + 0.68 to IW + 1.51; runs G403–G407) contain carbonate doublets at 1420 and 1510 cm^{-1}, which are absent for the sample glasses synthesized at relatively reduced conditions (IW − 0.39 to IW − 0.05; runs G408 and G409). All the spectra had a broad peak at ~3550 cm^{-1}, indicating the presence of OH^- in the glasses. The dissolved OH^- content and carbonate content were quantified using the Beer-Lambert law. The integrated molar extinction coefficient (Ɛ*) of 81,500 L mol^{-1} cm^{-2} determined by *Stanley et al.* [2011] for Humphrey Martian basalt and used in *Armstrong et al.* [2015] was used for quantifying the carbonate content. The molar extinction coefficient (Ɛ) of 78 L mol^{-1} cm^{-1} from *Jendrzejewski et al.* [1996] and used in *Armstrong et al.* [2015] for water at ~3550 cm^{-1} in Humphrey Martian basalt was used for quantifying the H_2O content. The results showed that the carbon contents in the form of carbonate for the oxidized glasses (runs G403–G407) were ~90–2400 ppm, and the OH^- (expressed as H_2O) contents in all the silicate glasses ranged from ~0.04 to 0.3 wt %, which are systematically lower than the corresponding bulk H_2O contents determined by SIMS (see Table 2).

4.4. Carbon Solubility in Silicate and Fe-Ni-C Melts and $D_C^{metal/silicate}$

The carbon solubility data in silicate melt and Fe-Ni-C melt are tabulated in Table 2. The carbon solubility in silicate melt determined by SIMS for all the runs ranges from 21 to 1388 ppm and increases with increasing oxygen fugacity (Figure 3 and Table 2). The correlation between carbon solubility in silicate melt and oxygen fugacity can be described as

$$\log C\ (\text{ppm}) = 0.97 \times \log fO_2(\Delta\text{IW}) + 1.61\ \left(R^2 = 0.99\right) \quad (3)$$

A comparison between the bulk carbon determined by SIMS, carbon as carbonate determined by FTIR, and the carbonate carbon calculated using the model of *Stanley et al.* [2011] and *Holloway et al.* [1992] is also provided in Figure 3 and Table 2. At the most oxidized conditions (IW + 1.24 to IW + 1.51; runs G403 and G404), the carbonate carbon determined by FTIR is about 2 times higher than the bulk carbon determined by SIMS, whereas at the intermediate oxygen fugacity (IW + 0.68 to IW + 0.72; runs G405 and G407), the carbonate carbon determined by FTIR is only about half of the bulk carbon determined by SIMS. At the most reduced conditions (IW − 0.39 to IW − 0.05; runs G408 and G409), the bulk carbon determined by SIMS is about 20–30 ppm; however, no carbonate was detected by FTIR even though the samples were prepared to be as thick as 300 μm. The disparity of the SIMS data and FTIR data could possibly be caused by the relatively high detection limit of FTIR and the used extinction coefficient, which was obtained from basaltic melts containing 1–3 wt % CO_2 [*Stanley et al.*, 2011]. The carbonate carbon calculated using the models of *Holloway et al.* [1992] and *Stanley et al.* [2011] is systematically lower than the bulk carbon determined by SIMS by a factor of 2–4 (Figure 3 and Table 2). The reason for which will be discussed below.

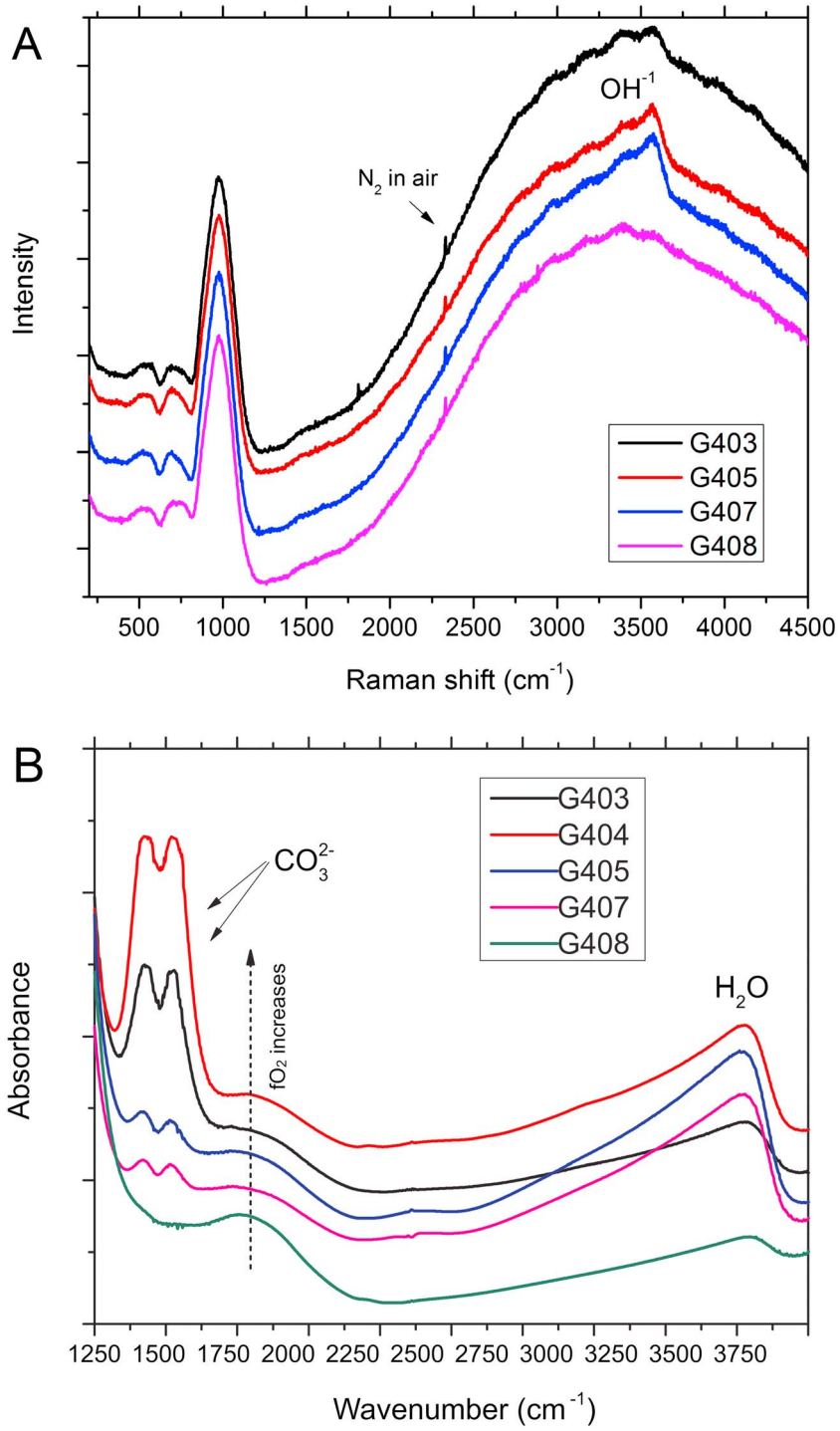

Figure 2. Representative (a) Raman and (b) FTIR spectra of experimental silicate glasses from this study showing regions associated with C–H–O species. See Table 2 for detailed experimental *P-T-f*O_2 conditions. Note that in the Raman spectra (Figure 2a), no peaks that can be ascribed to methane, iron carbonyl, or C≡O were observed. Also note that in the FTIR spectra (Figure 2b), only carbonate peaks were observed and the relative intensity of these peaks increases with increasing oxygen fugacity.

The carbon solubility in Fe-Ni-C melt is between 3.2 and 5.7 wt % (Table 2). The partition coefficient of carbon between Fe-Ni-C melt and silicate melt ($D_C^{metal/silicate}$) was calculated based on the measured carbon contents in alloy melt and silicate melt. The $D_C^{metal/silicate}$ values in this study varied from 23 to 2300, decreasing with

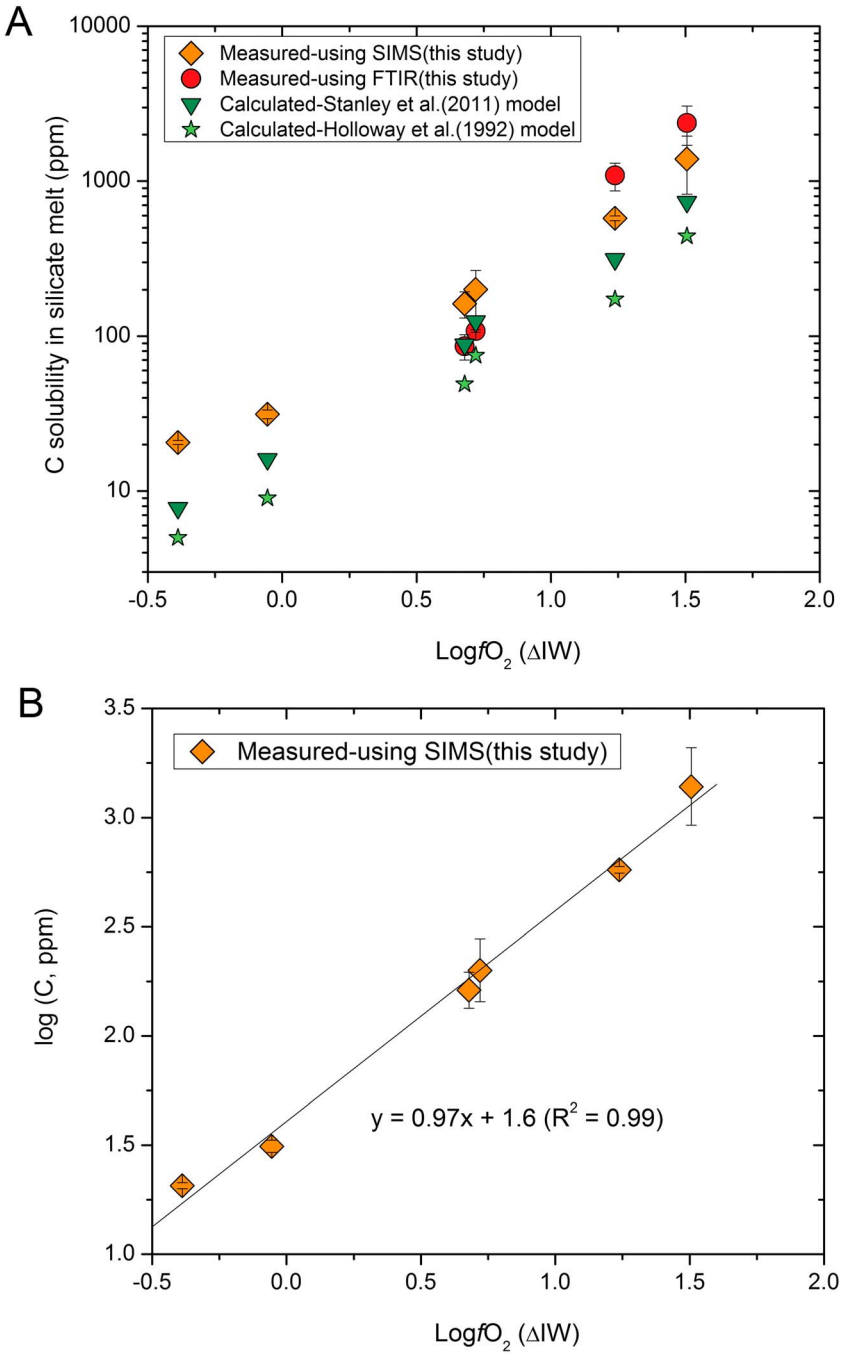

Figure 3. Carbon solubility in Martian basaltic melt determined in this study plotted as a function of logfO_2 (ΔIW). (a) The carbon content determined using FTIR and SIMS from this study compared with carbon solubility at graphite saturation calculated using the previous model of *Holloway et al.* [1992] for Hawaiian tholeiitic basalt and the model of *Stanley et al.* [2011] for Martian Humphrey basalt. (b) Log C (ppm) versus logfO_2 (ΔIW) plot showing that the slope of our experimental carbon solubility data is 0.97, which indicates that the main carbon species in the Martian basaltic melt studied here is carbonate (CO_3^{2-}). LogfO_2 values plotted in this figure are based on nonideal solution model of Fe and FeO in alloy melt and silicate melt, respectively, as tabulated in Table 2. See text for more details.

increasing oxygen fugacity. The $D_C^{metal/silicate}$ measured here at fO_2 below the IW buffer are consistent with those data in previous studies [e.g., *Chi et al.*, 2014; *Li et al.*, 2015, 2016], but no previous studies report any $D_C^{metal/silicate}$ data at fO_2 above the IW buffer.

5. Discussion

5.1. Carbon Dissolution in Reduced Mafic Silicate Melts

Previous spectroscopic studies show that carbon is dissolved mainly as carbonate in mafic melt at fO_2 around FMQ ± 2 [*Holloway et al.*, 1992; *Stanley et al.*, 2011; *Ni and Keppler*, 2013; *Duncan and Dasgupta*, 2014; *Duncan et al.*, 2017]. However, the carbon speciation in reduced mafic melt with logfO_2 below IW + 2 remains quite debated [*Kadik et al.*, 2004; *Dasgupta et al.*, 2013b; *Wetzel et al.*, 2013; *Stanley et al.*, 2011, 2014; *Chi et al.*, 2014; *Li et al.*, 2015; *Yoshioka et al.*, 2015; *Armstrong et al.*, 2015; *Li et al.*, 2016]. *Kadik et al.* [2004] suggested that atomic carbon or amorphous carbon, and Si-C complex might exist in their silicate melt with 1–2 wt % H_2O and logfO_2 of ~IW − 2.3, which, however, have never been confirmed by any other studies. *Wetzel et al.* [2013] assigned the Raman peak at 2110 cm^{-1} to be iron carbonyl [$(Fe(CO)_5$] dissolved in lunar basaltic melt with around 0.5 wt % water and logfO_2 below IW − 0.5. *Dasgupta et al.* [2013b], *Chi et al.* [2014], *Li et al.* [2015], and *Li et al.* [2016] showed coexisting carbonate and methane and probably other hydrogenated carbon species but no iron carbonyl in basaltic melt with ~0.4–2.0 wt % water and logfO_2 below IW − 0.4. *Stanley et al.* [2014] showed that their basaltic melt with ~0.4 wt % water does not contain hydrogenated carbon but probably iron carbonyl or C≡O bearing species at logfO_2 between IW − 0.3 and IW − 0.8. However, *Yoshioka et al.* [2015] show that the Raman peak at 2110 cm^{-1} is also present in the basaltic melt free of FeO, which strongly suggests that the peak at 2110 cm^{-1} cannot be assigned to iron carbonyl. Therefore, *Armstrong et al.* [2015] proposed that the noncarbonate carbon in their basaltic melts at logfO_2 of IW − 1 to IW + 1.7 may be mainly as C≡O.

Our six new experiments presented here allow us to reassess the speciation of carbon in reduced basaltic melt. The dissolution of carbon in silicate melt at graphite saturation can be described as

$$C\ (\text{graphite}) + ½\ O_2 = CO\ (\text{silicate}) \tag{4}$$

$$C\ (\text{graphite}) + O_2 + O^{2-}(\text{silicate}) = {CO_3}^{2-}(\text{silicate}) \tag{5}$$

$$H_2O\ (\text{silicate}) = H_2 + ½\ O_2 \tag{6}$$

$$C\ (\text{graphite}) + 2H_2 = CH_4(\text{silicate}) \tag{7}$$

The equilibrium constant of equation (4) can be written as

$$K_4 = fCO/(fO_2)^{1/2} \tag{8}$$

Equation (8) can be arranged as

$$\log fCO = \log K_4 + ½\ \log fO_2 \tag{9}$$

At a given P and T condition, equation (9) can be rearranged as

$$\log(C, \text{ppm}) = ½\ \log fO_2 + a \tag{10}$$

Similarly, the following equation can also be derived from equation (5).

$$\log(C, \text{ppm}) = \log fO_2 + b \tag{11}$$

In equations (10) and (11), C is carbon solubility in silicate melt, in ppm, and a and b are constants. Equation (10) implies that if carbon is dissolved mainly as C≡O in silicate melt, then log (C, ppm) should increase with ½ logfO_2. Equation (11) implies that if carbon is dissolved mainly as carbonate in silicate melt, then log (C, ppm) should increase with logfO_2. If carbon dissolution in silicate melt is both as C≡O and as CO_3^{2-} and if CH_4 is not present, then log (C, ppm) should increase with x logfO_2, where x is between 0.5 and 1. The fitting of our six data points yields a slope of 0.97 (Figure 3b). This therefore strongly suggests that the main carbon species in our basaltic melt is as CO_3^{2-}, rather than C≡O or other carbon species, consistent with our Raman and FTIR measurements (Figure 2).

Equations (6) and (7) suggest that a considerable amount of CH_4 could be dissolved in silicate melt, if melt H_2O content is sufficiently high and fO_2 is sufficiently low, as observed in our previous studies [*Dasgupta et al.*, 2013b; *Chi et al.*, 2014; *Li et al.*, 2015, 2016]. However, *Li et al.* [2015] showed that a considerable amount of CH_4 can only be present in the basaltic melt with logfO_2 below IW − 0.6 and melt H_2O content of 0.22–0.55 wt %. At 1600°C and 3 GPa, even though the melt H_2O content is about 0.19 wt % and logfO_2 is

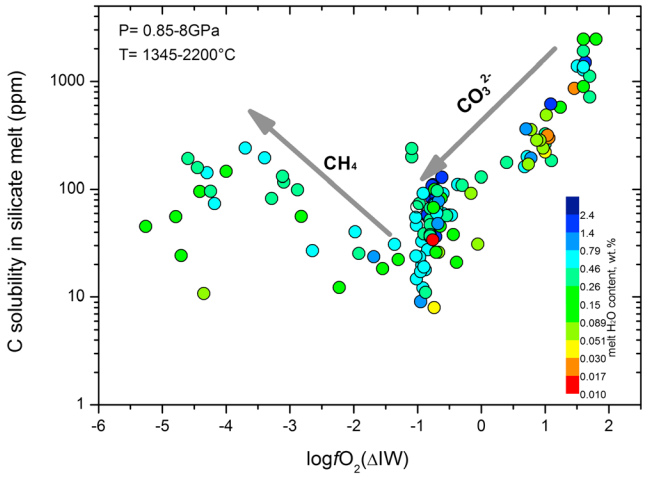

Figure 4. The carbon solubility in silicate melt at graphite saturation as a function of oxygen fugacity and melt H_2O content. Note that the solution behavior of carbon, based on the compiled studies, seem to change at logfO_2 of ~IW − 1. We postulate that this change is mostly due to the change of carbon species with oxygen fugacity and melt H_2O content. At logfO_2 above IW − 1, the main carbon species in silicate melt is carbonate, which decreases with decreasing oxygen fugacity, while at logfO_2 below IW − 1, the main carbon species is methane, which increases with decreasing oxygen fugacity and melt H_2O content. All the data used here are tabulated in Table S1.

as low as IW − 2.2, only about 12 ppm CH_4 was present in the basaltic melt [*Li et al.*, 2015]. Therefore, if any CH_4 is present in the basaltic melts of the relatively reduced runs G408 (0.09 wt % H_2O; logfO_2 of IW − 0.05) and G409 (0.09 wt % H_2O; logfO_2 of IW − 0.39), it should be negligible. This notion is consistent with the Raman measurements that document no signs of carbonyl complexes or C≡O and also the slope of 0.97 in the log(C, ppm) − logfO_2 plot (Figure 3b). Accordingly, our conclusion is that the carbon species dissolved in our basaltic melts is nearly pure carbonate at logfO_2 of IW − 0.39 to IW + 1.51 and at the *P-T* range studied. However, it should be noted that the presence of only carbonate in our two low H_2O and reduced runs G408 and G409 does not mean the absence of CH_4 in the silicate melt at similar *P-T-*fO_2 but with higher H_2O content.

5.2. A Model to Predict Carbon Solubility in Reduced Mafic Silicate Melts

As shown previously, the carbon content in reduced Martian basalt measured by SIMS is 2–4 times higher than that calculated using the models of *Holloway et al.* [1992] and *Stanley et al.* [2011]. The main reason for this difference may be due to the fact that both previous models were calibrated on the CO_2 solubility in a single Hawaiian tholeiitic basalt or Martian Humphrey basalt at oxidized conditions. Therefore, the application of these two models to a different mafic melt at reduced conditions may lead to large errors. Thus, one important goal of this study is to develop a model that can be used to predict carbon solubility in reduced mafic silicate melts generated by partial melting of the Martian mantle, the Mercurian mantle, and the lunar mantle. So far, a number of studies have investigated the carbon solubility in terrestrial mid-ocean ridge and alkaline basalts, in lunar basalts, in Martian basalts, and Mercurian mantle melt-like, FeO-poor mafic silicate melts at pressures of 0.85 to 8 GPa, temperatures of 1345 to 2200°C, and logfO_2 of IW − 5.3 to IW + 1.7 [*Dasgupta et al.*, 2013b; *Wetzel et al.*, 2013; *Chi et al.*, 2014; *Stanley et al.*, 2014; *Li et al.*, 2015; *Armstrong et al.*, 2015; *Li et al.*, 2016; *Duncan et al.*, 2017]. We will therefore take advantage of these available studies together with this study where we extended our experiments to relatively oxidizing conditions, to develop an empirical model that can be widely used to model carbon contents in the mantle partial melts of Mars, Mercury, and the Moon at graphite saturation. We note that in developing the models for carbon solubility at graphite saturation for mafic melts in this study we did not include recent experimental studies of graphite-saturated carbon solubility for more silicic melts where molecular CO_2 is also a key dissolved species [*Eguchi and Dasgupta*, 2017; *Duncan and Dasgupta*, 2017].

Table S1 in the supporting information and Figure 4 show all the previous graphite-saturated carbon solubility data along with our new data as a function of oxygen fugacity and melt H_2O content. As shown in Figure 4, the carbon solubility in mafic melts is a strong function of oxygen fugacity. At logfO_2 above IW − 1, the carbon solubility decreases significantly with decreasing oxygen fugacity, while at logfO_2 below IW − 1, the carbon solubility increases with decreasing oxygen fugacity and increasing melt H_2O content. The main reason for the variation of carbon solubility with oxygen fugacity and melt H_2O content is that at logfO_2 above IW − 1, the main carbon species in silicate melt is carbonate, the dissolution of which decreases with decreasing oxygen fugacity (equation (5)), whereas at logfO_2 below IW − 1, the main carbon species in

silicate melt is methane, the dissolution of which increases with decreasing oxygen fugacity and increasing melt H_2O content (equations (6) and (7)). In addition to oxygen fugacity and melt H_2O content, other factors can also affect carbon solubility. Increasing pressure may decrease the carbon content in graphite-saturated mafic silicate melt, while increasing temperature would increase the carbon solubility in mafic silicate melt [*Dasgupta et al.*, 2013b; *Chi et al.*, 2014; *Duncan et al.*, 2017]. The silicate melt composition may also significantly affect graphite-saturated carbon content [*Iacono-Marziano et al.*, 2012; *Dasgupta et al.*, 2013a; *Duncan et al.*, 2017]. We here use NBO/T (NBO/T = 2 total O/T − 4; T = Si + Ti + Al + Cr + P) to express the variation of mafic silicate melt composition, which may be appropriate as long as our model is restricted to broadly basaltic compositions [*Duncan et al.*, 2017]. In addition, at oxidizing conditions, the presence of H_2O may cause melt depolymerization and thus the enhancement of carbonate solubility in silicate melt [*Duncan and Dasgupta*, 2014]. Taking all of these factors into consideration and using all the previous carbon solubility data (Table S1 and Figure 4) obtained at conditions relevant for partial melting of the Martian mantle, the Mercurian mantle, and the lunar mantle, two empirical equations were derived in order to predict carbon solubility in reduced mantle melts:

$$\begin{aligned}&\text{At IW} + 1.7 \geq \log fO_2 \geq \text{IW} - 1:\\ &\log(\text{C, ppm}) = -3702(\pm534)/T - 194(\pm49)P/T - 0.0034(\pm0.043)\log X_{H2O}\\ &+0.61(\pm0.07)\text{NBO/T}\\ &+0.55(\pm0.02)\Delta\text{IW} + 3.5(\pm0.3)\ \left(R^2 = 0.89\right)\end{aligned} \tag{12}$$

$$\begin{aligned}&\text{At IW} - 5.3 \leq \log fO_2 \leq \text{IW} - 1:\\ &\log(\text{C, ppm}) = -2179(\pm1626)/T + 74(\pm76)P/T + 0.89(\pm0.16)\log X_{H2O}\\ &+0.035(\pm0.46)\text{NBO/T} - 0.26(\pm0.06)\Delta\text{IW}\\ &+3.6(\pm0.86)\ \left(R^2 = 0.74\right)\end{aligned} \tag{13}$$

in which T is temperature in K, P is pressure in GPa, X_{H2O} is mole fraction of water in silicate melt, and ΔIW is the oxygen fugacity relative to the Fe-FeO buffer. Equation (12) indicates that the increase of temperature, NBO/T, and oxygen fugacity would result in the increase of carbon solubility in mafic silicate melt, whereas the increase of pressure would result in the decrease of carbon solubility in mafic silicate melt. The effect of water remains to be a large uncertainty, which implies the insignificant effect of melt water on carbon solubility at graphite saturation at $\log fO_2 \geq \text{IW} - 1$. The coefficient of 0.55 for the oxygen fugacity term (ΔIW) may mean that besides carbonate, other carbon species such as methane or other reduced species may also be present in the silicate melt, particularly at high melt H_2O content in the previous studies [*Dasgupta et al.*, 2013b; *Chi et al.*, 2014; *Li et al.*, 2016; *Wetzel et al.*, 2013], although carbonate is the dominant carbon species in the experiments of this study. Equation (13) indicates that at $\log fO_2 \leq \text{IW} - 1$, melt water content and oxygen fugacity play a significant role in controlling carbon solubility in mafic silicate melt, while the effects of pressure, temperature, and melt composition (NBO/T) appear to be negligible, which thus leads us to fit all the data obtained at $\log fO_2 \leq \text{IW} - 1$ without taking pressure, temperature, and melt composition into account:

$$\begin{aligned}&\text{At IW} - 5.3 \leq \log fO_2 \leq \text{IW} - 1:\\ &\log(\text{C, ppm}) = 0.96(\pm0.19)\log X_{H2O} - 0.25(\pm0.04)\Delta\text{IW} + 2.83(\pm0.34)\ \left(R^2 = 0.6\right)\end{aligned} \tag{14}$$

Figure 5 shows how well equations (12) and (14) can capture the variability of the experimentally measured log(C, ppm) in mafic silicate melt. In the following sections, we will apply our empirical model to predict the carbon content in reduced planetary mantle melts at graphite saturation.

5.3. Applications to the Degassing of Reduced Planetary Mantles

5.3.1. Carbon Degassing of the Martian Mantle

The evidence in support of the presence of liquid water on the Martian surface during the late Noachian and Hesperian epochs requires that a significant amount of greenhouse gasses existed in the Martian atmosphere [*Carr*, 1999; *Kasting*, 1997; *Mangold et al.*, 2004; *Ramirez et al.*, 2014; *Squyres et al.*, 2004]. A highly likely candidate for these greenhouse gasses is CO_2 [*Carr*, 1999; *Jakosky and Phillips*, 2001], with other gasses such as SO_2, H_2, and CH_4 proposed as well [*Ding et al.*, 2014, 2015; *Halevy et al.*, 2007; *Ramirez et al.*, 2014; *Righter et al.*, 2009]. Similar to that in the Earth, a large fraction of Martian atmosphere may have been formed and maintained on long time scales by degassing of the mantle via partial melting. A few previous studies have

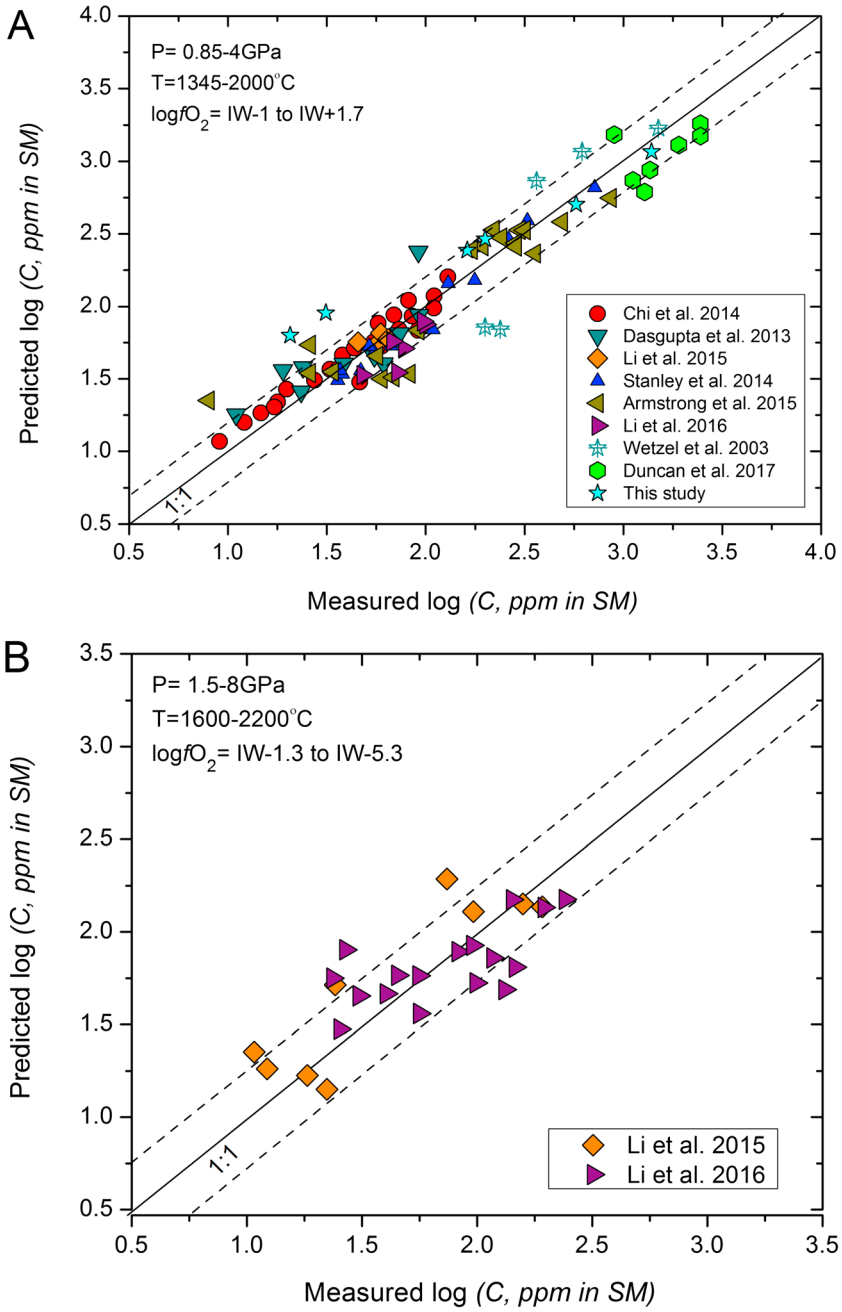

Figure 5. Comparison of the experimentally measured C (in ppm) versus predicted C (in ppm) in basaltic silicate melt (SM) using (a) equation (12) and (b) equation (14), i.e., at logfO_2 > IW − 1 and logfO_2 < IW − 1, respectively. The dashed lines in Figures 5a and 5b correspond to the 1σ error of our regression, 0.18 and 0.24, respectively.

estimated the quantity of CO_2 released from the Martian mantle during the formation of Martian crust [*Hirschmann and Withers*, 2008; *Stanley et al.*, 2011, 2012, 2014]. However, these studies always assumed that graphite is saturated during partial melting of the Martian mantle, considering the relatively low fO_2 of the Martian mantle [*Wadhwa*, 2008]. Moreover, the model used in these previous studies for predicting carbon solubility in the Martian mantle melt was established on the CO_2 solubility in Martian basalts at oxidized, vapor-present conditions [e.g., *Stanley et al.*, 2011]; however, as shown previously, this model appears to underestimate carbon solubility in the Martian basalts measured here at reduced conditions. Most importantly, carbon content (as CO_2 or as bulk C) of graphite-saturated Martian basalts are estimated

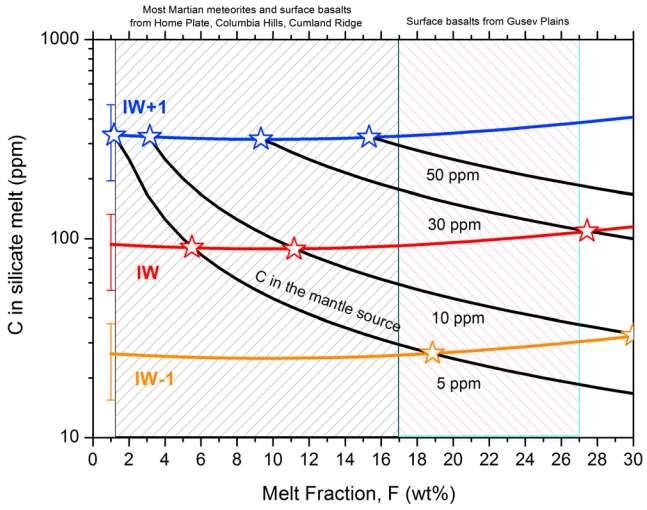

Figure 6. Carbon concentration in Martian basaltic melt as a function of degree of partial melting and carbon abundance in the mantle source. The blue, red, and orange curves are the calculated carbon solubility in Martian basaltic melts at three different oxygen fugacities. The degree of partial melting, and the corresponding *P-T* and melt composition were based on the melt composition-melt fraction data obtained at 1.5 GPa by *Bertka and Holloway* [1994]. The black curves represent dilution of the melt carbon content after the exhaustion of graphite for bulk Martian mantle with 5–50 ppm carbon. The cross between the black curves and other carbon solubility curves, as indicated by the star, refers to the point at which graphite is exhausted at certain oxygen fugacity and extent of melting. For example, at logfO_2 of IW and 10 ppm carbon in the mantle source, about 11% melting of the Martian mantle could result in graphite undersaturation. The dashed bands refer to the possible degree of partial melting estimated for different Martian basalts [*Filiberto and Dasgupta*, 2011] and indicate that many Martian basalts may have been produced at graphite undersaturation. The error bars show the errors of calculated carbon solubility at three different oxygen fugacities.

at high *P-T* for a couple of specific melt compositions and composition-based model for estimating carbon content of graphite-saturated mafic magmas of variable compositions is scarce and thus far only been constructed for terrestrial basalt-peridotite join and not for exploring full compositional spectrum within high- to low-FeO basalts [*Duncan et al.*, 2017]. Below we use our new model to discuss whether graphite is saturated during partial melting of the Martian mantle and also to discuss the maximum CO_2 that can be released during the Martian magmatic crust production process.

If graphite is saturated in the Martian mantle during the extraction of basaltic melt, the carbon content in the basaltic melt can be constrained by carbon content in the basaltic melt at graphite saturation, as long as the melt composition, the *P-T* conditions of melting, and the fugacity of oxygen are known. However, depending on the degree of melting and the bulk abundance of carbon in the Martian mantle, graphite could be exhausted during partial melting. Figure 6 shows the variation of carbon content in basaltic melt as a function of carbon abundance in the Martian mantle, and the degree of mantle melting. As the carbon abundance in the Martian mantle remains largely unknown [*Filiberto et al.*, 2016], a range of 5–50 ppm carbon was used in the calculation (Figure 6). The high end of these values is sufficiently higher than the carbon abundance constrained for the Martian mantle [*Grady et al.*, 2004; *Grady and Wright*, 2006; *Chi et al.*, 2014]. In Figure 6, the degree of melting, and the corresponding *P-T* conditions and melt compositions are based on the melt composition-melt fraction data obtained at 1.5 GPa by *Bertka and Holloway* [1994]. The carbon content at graphite saturation was calculated at three different oxygen fugacities, using equation (12). It can be seen from Figure 6 that at logfO_2 of IW + 1, 3% melting would exhaust all the graphite if the carbon abundance in the mantle source is 10 ppm, and 15% melting would exhaust all the graphite if the carbon abundance is 50 ppm. However, at logfO_2 of IW − 1, graphite would always be saturated during the generation of Martian basalts, if the carbon abundance in the mantle source is no less than 10 ppm. This is mainly due to the very low carbon solubility in the Martian basaltic melt. Carbon is highly incompatible in silicate minerals [*Rosenthal et al.*, 2015; *Shcheka et al.*, 2006] but highly compatible in alloy melt [*Chi et al.*, 2014; *Dasgupta et al.*, 2013b; *Li et al.*, 2015, 2016]. Therefore, the Martian mantle after core formation and solidification of the magma ocean may be significantly depleted in carbon. *Chi et al.* [2014] showed that $<$0.5 ppm carbon would be left in the Martian mantle after core-mantle separation, even if 3000 ppm carbon participated in core-mantle equilibrium in a magma ocean. *Grady and Wright* [2006] estimated a mantle carbon abundance of 4 ppm by analyzing Martian meteorites. Accordingly, it is highly likely that the Martian mantle carbon abundance is much less than that of the Earth [*Grady and Wright*, 2006], and a considerable fraction of Martian basalts may have been generated by partial melting in the absence of graphite saturation, in particular at logfO_2 of IW to IW + 1.

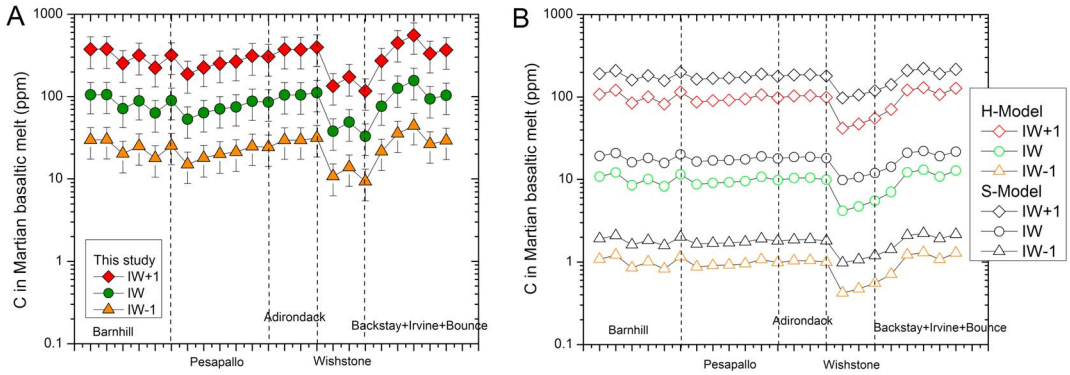

Figure 7. The calculated carbon content of 22 fractionation-corrected, graphite-saturated basaltic melts provided in *Filiberto and Dasgupta* [2011], using (a) equation (12) and using the (b) models of *Holloway et al.* [1992] and *Stanley et al.* [2011]. Note that the calculated carbon content based on equation (12) is higher than that based on the models of *Holloway et al.* [1992] and *Stanley et al.* [2011], in particular at reduced conditions. The main reason for this difference could be the fact that both models of *Holloway et al.* [1992] and *Stanley et al.* [2011] were calibrated on CO_2 solubility in an oxidized basaltic melt of a single composition, without taking the effects of melt composition and other carbon species into account, whereas in equation (12), all the factors (P, T, melt H_2O, melt composition, and fO_2) that potentially affect the carbon solubility in reduced mafic silicate melt are included.

Assuming that the Martian mantle is always saturated with graphite during partial melting, the dissolved maximum carbon content in the Martian basalts can be calculated using equation (12). *Filiberto and Dasgupta* [2011] provided 22 fractionation-corrected Martian basaltic compositions and the corresponding generating *P-T* conditions, based on compositions of surface Martian basalts form different locations in Gusev crater and Bounce Rock in Meridiani Planum. For these 22 primitive Martian basaltic compositions, we have calculated their carbon solubility at logfO_2 of IW − 1, IW, and IW + 1. The results (Figure 7a) show that at logfO_2 of IW + 1, IW, and IW − 1, the carbon solubility in Martian basaltic melt is 302 ± 102 ppm, 85 ± 28 ppm, and 24 ± 8 ppm, respectively. These values are about 1–30 times higher than the carbon solubility calculated using the models of *Holloway et al.* [1992] and *Stanley et al.* [2011] (Figure 7b), consistent with the results presented in Figure 3 and Table 2. This could be ascribed to the variation of silicate melt composition and the presence of reduced carbon species in the presence of water and at low oxygen fugacity, because the models of *Holloway et al.* [1992] and *Stanley et al.* [2011] are based on CO_2 solubility in a single basaltic melt at oxidized conditions, without taking the effects of melt composition and water into account. Using these newly calculated values and the magmatic production model of *Hirschmann and Withers* [2008], the total volcanic outgassing of carbon as CO_2 was calculated for Mars from 4.5 Ga to the present (Figure 8). The calculations in Figure 8 assumed that all the carbon degassed into the atmosphere was eventually converted into CO_2 and no CO_2 was removed from the atmosphere, although CH_4 and/or CO may also degas directly into the atmosphere [*Li et al.*, 2015; *Gaillard et al.*, 2012; *Gaillard et al.*, 2015; *Wetzel et al.*, 2013].

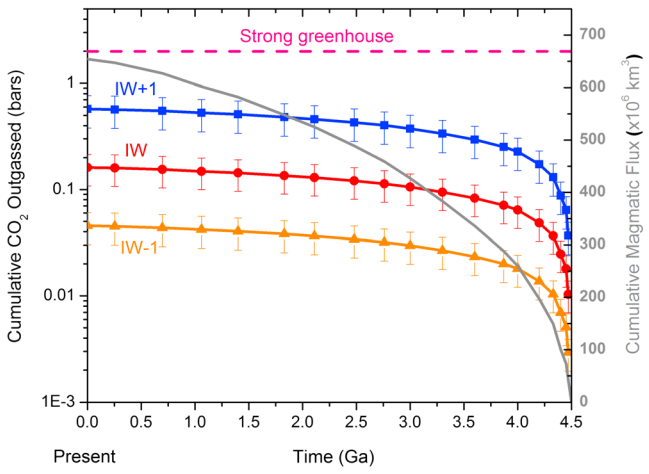

Figure 8. Total volcanic outgassing of CO_2 calculated for Mars from 4.5 Ga to the present, assuming that graphite is always saturated during mantle melt extraction. The cumulative magmatic flux (right y axis) was calculated using the magmatic production model of *Hirschmann and Withers* [2008]. The average values of carbon solubility in the 22 primitive Martian basaltic melt at logfO_2 of IW − 1 to IW + 1, shown in Figure 7a, are taken as the carbon solubility in the Martian basaltic melt involved in these calculations. The "strong greenhouse" of 2 bar, thought to be efficient to warm the early Mars, is based on *Pepin* [1994] and *Manning et al.* [2006].

Figure 8 shows that the cumulated CO_2 in the Martian atmosphere would be less than 0.1 bar if logfO_2 of the mantle source is IW − 1. At logfO_2 of IW, the cumulated CO_2 pressure is less than 0.2 bar, and at logfO_2 of IW + 1 the accumulated CO_2 pressure is less than 0.5 bar. Considering that at logfO_2 of IW to IW + 1, graphite may not be saturated during Martian mantle melting, the actual CO_2 released by Martian mantle should be considerably less than these values. Previous studies of *Pepin* [1994], *Carr* [1999], and *Manning et al.* [2006] argued that the CO_2 partial pressure in the atmosphere of Mars may need to be above 2 bars to work as a strong greenhouse gas. Therefore, the CO_2 released from the Martian mantle magmatic degassing alone cannot be sufficient to warm the early Mars. This conclusion is, in general, consistent with the conclusions of *Hirschmann and Withers* [2008] and *Stanley et al.* [2011, 2012], which show that the maximum CO_2 partial pressure in the Martian atmosphere may reach up to 1 bar.

In the case graphite is exhausted during Martian mantle melting, the total CO_2 flux during generation of the Martian crust can also be calculated. For example, at logfO_2 of IW and 14% degree of mantle melting in average, the cumulated CO_2 in the atmosphere during the past 4.5 billion years would be about 0.004 bar and 0.008 bar, respectively, if we assume 5 and 10 ppm carbon in the Martian mantle.

5.3.2. Carbon Degassing of the Lunar Mantle

Several volatiles including CO, H_2, H_2O, and SO_2 have been suggested to be the potential propellant for lunar fire-fountain eruptions; however, which volatile is the main propellant is still under debate [*McCubbin et al.*, 2015]. A number of studies have proposed that CO, produced likely by graphite oxidation at shallow depth, could be the main propellant [*Fogel and Rutherford*, 1995; *Nicholis and Rutherford*, 2009; *Rutherford and Papale*, 2009]. However, graphite has never been found in lunar materials. Most recently, *Wetzel et al.* [2015] estimated a carbon content of 40–60 ppm in lunar basaltic melt inclusion hosted by olivine of the pyroclastic glass, suggesting again that CO_2/CO could be the main volatile driving fire-fountain eruptions. However, so far only very limited data of carbon content in lunar basaltic melt are available, which hampers our full understanding of the role of carbon in lunar fire-fountain eruptions. The model presented above allows for assessing the carbon degassing of the lunar mantle by partial melting and the role of carbon in lunar fire-fountain eruptions. The oxygen fugacity of the lunar mantle may be between IW − 2 and IW [*Nicholis and Rutherford*, 2009; *Wadhwa*, 2008]. At given *P-T-fO*$_2$ conditions of the lunar mantle, the above model shows that the maximum carbon content in partial melts of the lunar mantle can be achieved at graphite saturation. Using three representative compositions of high-TiO_2, low-TiO_2, and very low TiO_2 picritic glasses (corresponding to the lunar orange, yellow, and green glasses, respectively) and using the estimated *P-T* conditions for generating picritic melt in the lunar mantle [*Shearer et al.*, 2006, Tables 4.6 and 4.9, and references therein], the carbon solubility in the lunar picritic melts were calculated at three different oxygen fugacities (Figure 9). Figure 9 illustrates that about 40–200 ppm carbon could be dissolved in the silicate melt at logfO_2 of IW, which is similar to the values estimated by *Wetzel et al.* [2015]. However, at IW − 1 and IW − 2, the calculated carbon in the silicate melt is about 10 to 60 ppm and 9 ppm, respectively. Therefore, if the values estimated by *Wetzel et al.* [2015] are correct and representative, this indicates that the logfO_2 of the lunar mantle may be between IW − 1 and IW, not down to IW − 2, and the lunar mantle may be graphite saturated during melt extraction. However, if the lunar mantle oxygen fugacity is down to IW − 2, then *Wetzel et al.* [2015] may have overestimated the carbon content in the lunar picritic melt and carbon from the mantle cannot be one important propellant for lunar fire-fountain eruptions. Furthermore, if the lunar mantle oxygen fugacity is higher than IW, the values estimated by *Wetzel et al.* [2015] may indicate that the lunar mantle may not be saturated with graphite during melt extraction.

5.3.3. Carbon Degassing of the Mercurian Mantle

One important finding from the MErcury Surface, Space ENvironment, GEochemistry, and Ranging (MESSENGER) spacecraft is that widespread volcanism existed on the surface of Mercury [*Head et al.*, 2011, 2008; *Marchi et al.*, 2013; *Thomas et al.*, 2014]. Similar to the fire-fountain eruptions on the Moon, explosive volcanism on the Mercury would also need volatiles such as CO, CO_2, H_2O, SO_2, and/or H_2S at the concentration level of hundreds to thousands of parts per million [*Kerber et al.*, 2009; *Thomas et al.*, 2015; *Weider et al.*, 2016]. Based on the chemistry data of MESSENGER spacecraft, a number of recent studies have also found that the Mercurian mantle oxygen fugacity may be 3–6 log units below IW and the Mercurian crust may be significantly enriched in carbon and sulfur [*McCubbin et al.*, 2012; *Peplowski et al.*, 2016, 2015; *Zolotov*, 2011; *Zolotov et al.*, 2013; *Namur et al.*, 2016a] The graphite-rich crust could be formed by graphite flotation during the early magma ocean stage, due to the relatively low density of graphite and the extremely reduced

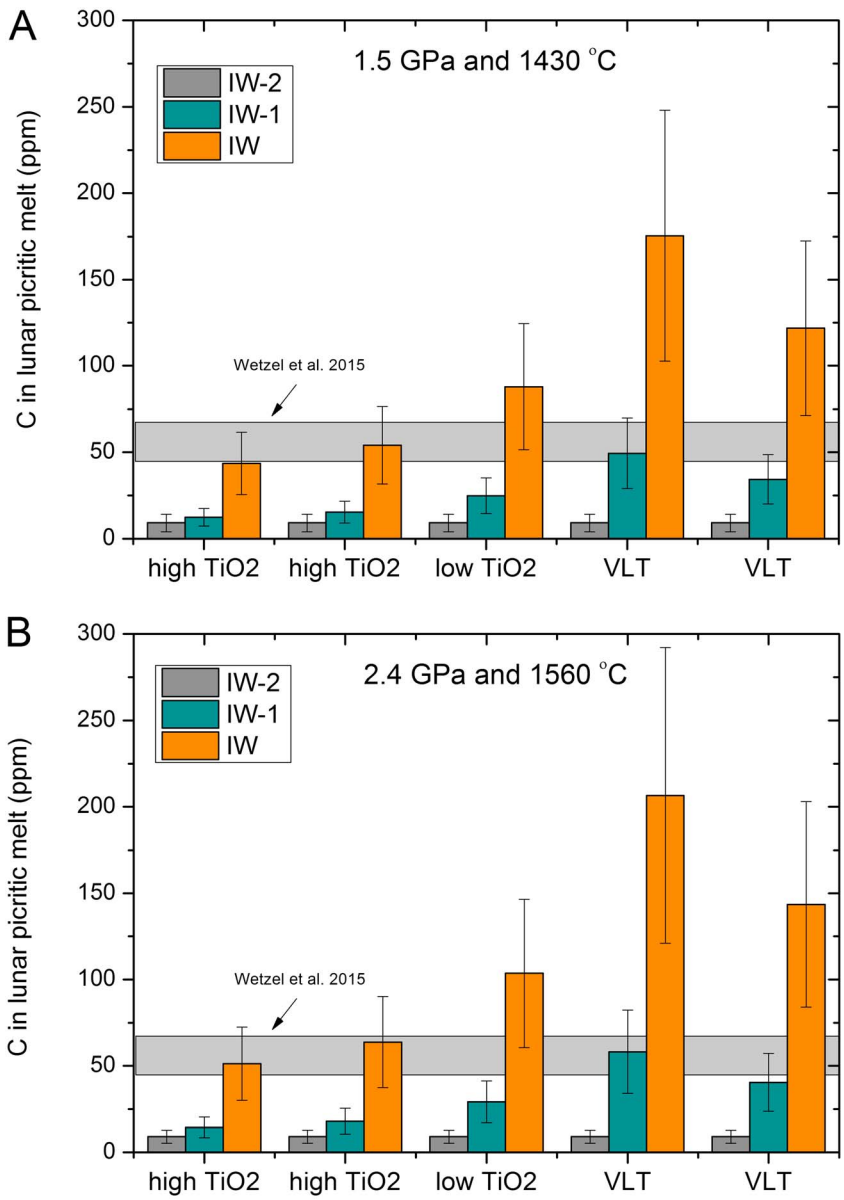

Figure 9. The calculated carbon content in graphite-saturated, lunar picritic melt as a function of oxygen fugacity, using equations (12) and (14). Three representative compositions of high-TiO_2, low-TiO_2, and very low TiO_2 (VLT) picritic glasses and the estimated *P-T* range for generating picritic melts in lunar mantle [*Shearer et al.*, 2006, Tables 4.6 and 4.9] were used. In Table 4.6 of *Shearer et al.* [2006], for the high-TiO_2 picritic melt and the very low TiO_2 picritic melt, two representative compositions with slightly different TiO_2 and FeO are given, which are also adopted here to show the effect of melt composition on the calculated carbon content. Note that the high-TiO_2, lot-TiO_2, and very low TiO_2 picritic glasses correspond to the average Apollo 14, 17 orange glasses; Apollo 15 yellow glasses; and Apollo 14, 16 green glasses, respectively. A H_2O content of 0.1 wt % was assumed in all the lunar picritic melts. The estimated carbon content (44–64 ppm) in lunar melt inclusions hosted by olivine in orange, yellow, and green glasses [*Wetzel et al.*, 2015] was plotted for comparison. Note that at logfO_2 between IW − 1 and IW, the estimated carbon content by *Wetzel et al.* [2015] can be reproduced.

conditions of Mercury where carbon would be expelled from the S- and Si-rich core [*Vander Kaaden and McCubbin*, 2015; *Li et al.*, 2016]. Whether the Mercurian mantle still contains graphite remains unknown, but it remains plausible that graphite was retained in the Mercurian mantle during the solidification of the Mercurian magma ocean. If this is the case, then partial melting of the Mercurian mantle or crust, responsible for the Mercurian volcanism, may have occurred at graphite saturation. To estimate how much

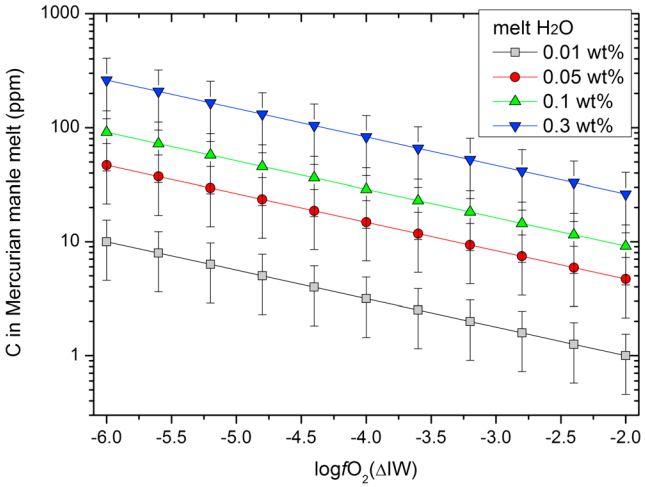

Figure 10. The calculated carbon content in graphite-saturated Mercurian mantle melt as a function of meltwater content and oxygen fugacity, using equation (14). See text for more details.

carbon can be transported by partial melts of the Mercurian mantle and to assess whether carbon-bearing fluids can be potential propellant responsible for the Mercurian explosive volcanism, we have calculated the carbon solubility in Mercurian lava-like silicate melt, using equation (14).

Considering the fact that equation (14) was derived based on many graphite-saturated experiments that produced extremely reduced, FeO-poor silicate melts [e.g., *Li et al.*, 2015, 2016], the composition and oxygen fugacity of which are similar to those of Mercurian mantle-derived lavas in the Northern Volcanic Plains and the high-Mg region of the Intercrater Plains and Heavily Cratered Terrains [*Malavergne et al.*, 2014; *Vander Kaaden and McCubbin*, 2015, 2016; *Zolotov et al.*, 2013; *Namur et al.*, 2016b], and considering that pressure and temperature play a negligible role in carbon solubility in very reduced silicate melt, we directly calculated the carbon solubility in Mercurian lavas as a function of oxygen fugacity and melt H_2O content, using equation (14). The calculated results are presented in Figure 10. It can be seen from Figure 10 that melt water plays an important role in controlling carbon solubility in Mercurian lavas. If the melt water content is $\leq$0.05 wt %, the carbon solubility would be $\leq$50 ppm. However, the carbon solubility may reach 300 ppm if the melt water content is 0.3 wt %. Moreover, it should be noted that in these reduced hydrous melt, the carbon is present as CH_4, rather than CO_2, as noted previously. Therefore, the capacity of partial melts of the Mercurian mantle in transporting deep carbon to the surface significantly depends on the water content in the mantle source region, at least if C–O–H is the chief volatiles. Hydrogen-bearing ionized molecules have been tentatively identified in the Mercurian surface by MESSENGER [*Zurbuchen et al.*, 2008]. However, these molecules may have resulted from solar wind or cometary/meteoritic impacts [*Zolotov*, 2011, and references therein]. Mercurian endogenic water may not be excluded, but *Zolotov* [2011] proposed that the Mercurian mantle is likely to be depleted in water, considering that water is the major oxidizing agent in planetary bodies and the fact that the Mercurian mantle is very reduced. If this is correct and if the partial melts of the Mercurian mantle contain less than 0.01 wt % water, then the carbon ($<$10 ppm) brought by the Mercurian mantle melts to the surface cannot be an important propellant for the explosive volcanism on Mercury. Considering that the Mercurian crust is enriched in graphite, the production of CO at shallow depth by graphite oxidation may be one mechanism for the driving of Mercurian explosive eruptions [*Weider et al.*, 2016]. However, whether the reaction between graphite and partial melts of such reduced Mercurian mantle can produce significant CO needs to be tested experimentally.

6. Conclusions

Our experiments yielded carbon content of 20–1400 ppm in graphite-saturated model Martian basalts at temperatures of 1400–1550°C, pressures of 1–2 GPa, and logfO_2 of IW − 0.4 to IW + 1.5. The carbon content in graphite-saturated Martian basalts is mainly controlled by fO_2 at the *P-T* range studied. This is confirmed by our Raman and FTIR measurements on the quenched silicate glasses, which show that carbonate is the only carbon species detected, with the previously proposed iron carbonyl or C≡O being not detectable.

By combining with the previous literature data on carbon solubility in reduced mafic silicate melt, empirical models (equations (12) and (14)) were developed to predict the carbon content in graphite-saturated basaltic melts. Our new model differs from previous models of *Holloway et al.* [1992] and *Stanley et al.* [2011] by including all the factors (*P*, *T*, melt H_2O, melt composition, and fO_2) that potentially affect

carbon solubility in reduced mafic silicate melts, i.e., rather than being applicable for a single melt composition. Application of this new model to partial melts of the Martian mantle, the Mercurian mantle, and the lunar mantle shows that graphite may not be saturated during the extraction of some Martian basalts, and the cumulative CO_2 in the atmosphere during the magmatic formation of the Martian crust is much less than 1 bar, implying that CO_2 cannot be an efficient greenhouse gas in the early Mars. At fO_2 corresponding to the lunar mantle, the lunar picritic melt can bring a few tens to 200 ppm carbon from the mantle source to surface, and this carbon as CO_2 may be one of the main propellant driving the fire-fountain eruption on the Moon. The carbon content in graphite-saturated Mercurian mantle melt is mainly controlled by water content in the melt. Considering that the Mercurian mantle may be very depleted in water [*Zolotov*, 2011], the capacity of the extremely reduced Mercurian mantle melt in transporting carbon may be very low. Consequently, the Mercurian mantle carbon may not be an important propellant for the explosive eruption on Mercury, although Mercury is a planet which may be quite rich in graphite. Our model, however, does not consider potential effects of other volatile species such as sulfur in affecting the graphite-saturated carbon solubility. Therefore, future studies should constrain the effects of high dissolved sulfur in reduced Mercurian partial melts on carbon solubility.

Acknowledgments
We gratefully acknowledge the formal reviews by Fabrice Gaillard and an anonymous reviewer. This work was supported by the Strategic Priority Research Program (B) of the Chinese Academy of Sciences (XDB18020301) to Y.L. and the NASA grant NNX13AM51G to R.D. All the carbon solubility data used for Figure 4 and the derivation of equation – are available in the supporting information.

References

Armstrong, L. S., M. M. Hirschmann, B. D. Stanley, E. G. Falksen, and S. D. Jacobsen (2015), Speciation and solubility of reduced C–O–H–N volatiles in mafic melt: Implications for volcanism, atmospheric evolution, and deep volatile cycles in the terrestrial planets, *Geochim. Cosmochim. Acta*, *171*, 283–302.

Bertka, C. M., and J. R. Holloway (1994), Anhydrous partial melting of an iron-rich mantle I: Subsolidus phase assemblages and partial melting phase relations at 10 to 30 kbar, *Contrib. Mineral. Petrol.*, *115*, 313–322.

Carr, M. H. (1999), Retention of an atmosphere on early Mars, *J. Geophys. Res.*, *104*, 21897–21909.

Chi, H., R. Dasgupta, M. S. Duncan, and N. Shimizu (2014), Partitioning of carbon between Fe-rich alloy melt and silicate melt in a magma ocean—Implications for the abundance and origin of volatiles in Earth, Mars, and the Moon, *Geochim. Cosmochim. Acta*, *139*, 447–471.

Dasgupta, R. (2013), Ingassing, storage, and outgassing of terrestrial carbon through geologic time, *Rev. Mineral. Geochem.*, *75*, 183–229.

Dasgupta, R., and D. Walker (2008), Carbon solubility in core melts in a shallow magma ocean environment and distribution of carbon between the Earth's core and the mantle, *Geochim. Cosmochim. Acta*, *72*, 4627–4641.

Dasgupta, R., A. Mallik, K. Tsuno, A. C. Withers, G. Hirth, and M. M. Hirschmann (2013a), Carbon-dioxide-rich silicate melt in the Earth's upper mantle, *Nature*, *493*, 211–215.

Dasgupta, R., H. Chi, N. Shimizu, A. S. Buono, and D. Walker (2013b), Carbon solution and partitioning between metallic and silicate melts in a shallow magma ocean: Implications for the origin and distribution of terrestrial carbon, *Geochim. Cosmochim. Acta*, *102*, 191–212.

Ding, S., R. Dasgupta, and K. Tsuno (2014), Sulfur concentration of Martian basalts at sulfide saturation at high pressures and temperatures—Implications for deep sulfur cycle on Mars, *Geochim. Cosmochim. Acta*, *131*, 227–246.

Ding, S., R. Dasgupta, C.-T. Lee, and M. Wadhwa (2015), New bulk sulfur measurements of Martian meteorites and modeling the fate of sulfur during melting and crystallization—Implications for sulfur transfer from Martian mantle to crust–atmosphere system, *Earth Planet. Sci. Lett.*, *409*, 157–167.

Duncan, M. S., and R. Dasgupta (2014), CO_2 solubility and speciation in rhyolitic sediment partial melts at 1.5–3.0 GPa—Implications for carbon flux in subduction zones, *Geochim. Cosmochim. Acta*, *124*, 328–347.

Duncan, M. S., and R. Dasgupta (2015), Pressure and temperature dependence of CO_2 solubility in hydrous rhyolitic melt: Implications for carbon transfer to mantle source of volcanic arcs via partial melt of subducting crustal lithologies, *Contrib. Mineral. Petrol.*, *169*(6), doi:10.1007/s00410-015-1144-5.

Duncan, M. S., and R. Dasgupta (2017), Rise of Earth's atmospheric oxygen controlled by efficient subduction of organic carbon, *Nat. Geosci.*, *10*, 387–392.

Duncan, M. S., R. Dasgupta, and K. Tsuno (2017), Experimental determination of CO_2 content at graphite saturation along a natural basalt-peridotite melt join: Implications for the fate of carbon in terrestrial magma oceans, *Earth Planet. Sci. Lett.*, *466*, 115–128, doi:10.1016/j.epsl.2017.03.008.

Eggler, D. H. (1978), The effect of CO_2 upon partial melting of peridotite in the system Na_2O-CaO-Al_2O_3-MgO-SiO_2-CO_2 to 35 kb, with an analysis of melting in a peridotite-H_2O-CO_2 system, *Am. J. Sci.*, *278*, 305–343.

Eguchi, J., and R. Dasgupta (2017), CO_2 content of andesitic melts at graphite saturated upper mantle conditions with implications for redox state of oceanic basalt source regions and remobilization of reduced carbon from subducted eclogite, *Contrib. Mineral. Petrol.*, *172*, 12, doi:10.1007/s00410-00017-01330-00418.

Filiberto, J., and R. Dasgupta (2011), Fe^{2+}–Mg partitioning between olivine and basaltic melts: Applications to genesis of olivine-phyric shergottites and conditions of melting in the Martian interior, *Earth Planet. Sci. Lett.*, *304*, 527–537.

Filiberto, J., and R. Dasgupta (2015), Constraints on the depth and thermal vigor of melting in the Martian mantle, *J. Geophys. Res. Planets.*, *120*, 109–122, doi:10.1002/2014JE004745.

Filiberto, J., R. Dasgupta, W. S. Kiefer, and A. H. Treiman (2010), High pressure, near-liquidus phase equilibria of the Home Plate basalt Fastball and melting in the Martian mantle, *Geophys. Res. Lett.*, *37*, L13201, doi:10.11029/12010GL043999.

Filiberto, J., D. Baratoux, D. Beaty, D. Breuer, B. Farcy, M. Grott, J. Jones, W. Kiefer, P. Mane, F. McCubbin, S. Schwenzer (2016), A review of volatiles in the Martian interior, *Meteorit. Planet. Sci.*, *51*(11), 1935–1958, doi:10.1111/maps.12680.

Fogel, R. A., and M. J. Rutherford (1995), Magmatic volatiles in primitive lunar glasses: I. FTIR and EPMA analyses of Apollo 15 green and yellow glasses and revision of the volatile-assisted fire-fountain theory, *Geochim. Cosmochim. Acta*, *59*, 201–215.

Frost, D. J., and C. A. McCammon (2008), The redox state of Earth's mantle, *Annu. Rev. Earth Planet. Sci.*, *36*, 389–420.

Gaillard, F., J. Michalski, G. Berger, S. M. McLennan, and B. Scaillet (2012), Geochemical reservoirs and timing of sulfur cycling on mars, *Space Sci. Rev.*, *174*(1–4), 251–300, doi:10.1007/s11214-012-9947-4.

Gaillard, F., B. Scaillet, M. Pichavant, and G. Iacono-Marziano (2015), The redox geodynamics linking basalts and their mantle sources through space and time, *Chem. Geol.*, *418*, 217–233, doi:10.1016/j.chemgeo.2015.07.030.
Grady, M., A. Verchovsky, and I. Wright (2004), Magmatic carbon in Martian meteorites: Attempts to constrain the carbon cycle on Mars, *Int. J. Astrobiol.*, *3*(02), 117–124.
Grady, M. M., and I. Wright (2006), The carbon cycle on early Earth—And on Mars?, *Phil. Trans. Roy. Soc. Lond. B: Biol. Sci.*, *361*(1474), 1703–1713.
Halevy, I., M. T. Zuber, and D. P. Schrag (2007), A sulfur dioxide climate feedback on early Mars, *Science*, *318*, 1903–1907.
Head, J. W., S. L. Murchie, L. M. Prockter, M. S. Robinson, S. C. Solomon, R. G. Strom, C. R. Chapman, T. R. Watters, W. E. McClintock, and D. T. Blewett (2008), Volcanism on Mercury: Evidence from the first MESSENGER flyby, *Science*, *321*, 69–72.
Head, J. W., C. R. Chapman, R. G. Strom, C. I. Fassett, B. W. Denevi, D. T. Blewett, C. M. Ernst, T. R. Watters, S. C. Solomon, and S. L. Murchie (2011), Flood volcanism in the northern high latitudes of Mercury revealed by MESSENGER, *Science*, *333*, 1853–1856.
Helo, C., M.-A. Longpré, N. Shimizu, D. A. Clague, and J. Stix (2011), Explosive eruptions at mid-ocean ridges driven by CO_2-rich magmas, *Nat. Geosci.*, *4*, 260–263.
Hirschmann, M. M., and A. C. Withers (2008), Ventilation of CO_2 from a reduced mantle and consequences for the early Martian greenhouse, *Earth Planet*, *Sci. Lett.*, *270*, 147–155.
Holloway, J. R., V. Pan, and G. Gudmundsson (1992), High-pressure fluid-absent melting experiments in the presence of graphite: Oxygen fugacity, ferric/ferrous ratio and dissolved CO_2, *Eur. J. Mineral.*, *4*, 105–114.
Holzheid, A., H. Palme, and S. Chakraborty (1997), The activities of NiO, CoO and FeO in silicate melts, *Chem. Geol.*, *139*, 21–38.
Iacono-Marziano, G., Y. Morizet, E. Le Trong, and F. Gaillard (2012), New experimental data and semi-empirical parameterization of H_2O–CO_2 solubility in mafic melts, *Geochim. Cosmochim. Acta*, *97*, 1–23, doi:10.1016/j.gca.2012.08.035.
Jakosky, B. M., and R. J. Phillips (2001), Mars' volatile and climate history, *Nature*, *412*, 237–244.
Jendrzejewski, N., M. Javoy, and T. Trull (1996), Quantitative measurements of water and carbon concentrations in natural basaltic glasses by infrared spectroscopy. 1. Carbon, *CR Acad. Sci. Ser. Fasc. Sci. Terre Planetes*, *322*, 645–652.
Kadik, A., F. Pineau, Y. Litvin, N. Jendrzejewski, I. Martinez, and M. Javoy (2004), Formation of carbon and hydrogen species in magmas at low oxygen fugacity, *J. Petrol.*, *45*, 1297–1310.
Kasting, J. F. (1997), Warming early Earth and Mars, *Science*, *276*, 1213.
Kerber, L., J. W. Head, S. C. Solomon, S. L. Murchie, D. T. Blewett, and L. Wilson (2009), Explosive volcanic eruptions on Mercury: Eruption conditions, magma volatile content, and implications for interior volatile abundances, *Earth Planet. Sci. Lett.*, *285*, 263–271.
Li, Y., R. Dasgupta, and K. Tsuno (2015), The effects of sulfur, silicon, water, and oxygen fugacity on carbon solubility and partitioning in Fe-rich alloy and silicate melt systems at 3 GPa and 1600°C: Implications for core–mantle differentiation and degassing of magma oceans and reduced planetary mantles, *Earth Planet. Sci. Lett.*, *415*, 54–66.
Li, Y., R. Dasgupta, K. Tsuno, B. Monteleone, and N. Shimizu (2016), Carbon and sulfur budget of the silicate Earth explained by accretion of differentiated planetary embryos, *Nat. Geosci.*, *9*(10), 781–785.
Ma, Z. (2001), Thermodynamic description for concentrated metallic solutions using interaction parameters, *Metall. Mater. Trans.B.*, *32,* 87–103.
Malavergne, V., M. J. Toplis, S. Berthet, and J. Jones (2010), Highly reducing conditions during core formation on Mercury: Implications for internal structure and the origin of a magnetic field, *Icarus*, *206*, 199–209.
Malavergne, V., et al. (2014), How Mercury can be the most reduced terrestrial planet and still store iron in its mantle, *Earth Planet. Sci. Lett.*, *394*, 186–197.
Mangold, N., C. Quantin, V. Ansan, C. Delacourt, and P. Allemand (2004), Evidence for precipitation on Mars from dendritic valleys in the Valles Marineris area, *Science*, *305*, 78–81.
Manning, C. V., C. P. McKay, and K. J. Zahnle (2006), Thick and thin models of the evolution of carbon dioxide on Mars, *Icarus*, *180*, 38–59.
Marchi, S., C. R. Chapman, C. I. Fassett, J. W. Head, W. Bottke, and R. G. Strom (2013), Global resurfacing of Mercury 4.0–4.1 billion years ago by heavy bombardment and volcanism, *Nature*, *499*, 59–61.
McCubbin, F. M., M. A. Riner, K. E. Vander Kaaden, and L. K. Burkemper (2012), Is Mercury a volatile-rich planet?, *Geophys. Res. Lett.*, *39*, L09202, doi:10.1029/2012GL051711.
McCubbin, F. M., K. E. V. Kaaden, R. Tartèse, R. L. Klima, Y. Liu, J. Mortimer, J. J. Barnes, C. K. Shearer, A. H. Treiman, and D. J. Lawrence (2015), Magmatic volatiles (H, C, N, F, S, Cl) in the lunar mantle, crust, and regolith: Abundances, distributions, processes, and reservoirs, *Am. Mineral.*, *100*, 1668–1707.
Musselwhite, D. S., H. A. Dalton, W. S. Kiefer, and A. H. Treiman (2006), Experimental petrology of the basaltic shergottite Yamato-980459: Implications for the thermal structure of the Martian mantle, *Meteorit. Planet. Sci.*, *41*(9), 1271–1290.
Mysen, B. O., K. Kumamoto, G. D. Cody, and M. L. Fogel (2011), Solubility and solution mechanisms of C–O–H volatiles in silicate melt with variable redox conditions and melt composition at upper mantle temperatures and pressures, *Geochim. Cosmochim. Acta*, *75*, 6183–6199.
Namur, O., B. Charlier, F. Holtz, C. Cartier, and C. McCammon (2016a), Sulfur solubility in reduced mafic silicate melts: Implications for the speciation and distribution of sulfur on Mercury, *Earth Planet. Sci. Lett.*, *448*, 102–114, doi:10.1016/j.epsl.2016.05.024.
Namur, O., M. Collinet, B. Charlier, T. L. Grove, F. Holtz, and C. McCammon (2016b), Melting processes and mantle sources of lavas on Mercury, *Earth Planet. Sci. Lett.*, *439*, 117–128.
Ni, H., and H. Keppler (2013), Carbon in silicate melts, *Rev. Mineral. Geochem.*, *75*, 251–287.
Nicholis, M. G., and M. J. Rutherford (2009), Graphite oxidation in the Apollo 17 orange glass magma: Implications for the generation of a lunar volcanic gas phase, *Geochim. Cosmochim. Acta*, *73*, 5905–5917.
O'Neill, H. S. C., and S. M. Eggins (2002), The effect of melt composition on trace element partitioning: An experimental investigation of the activity coefficients of FeO, NiO, CoO, MoO_2 and MoO_3 in silicate melts, *Chem. Geol.*, *186*, 151–181.
Pepin, R. O. (1994), Evolution of the Martian atmosphere, *Icarus*, *111*, 289–304.
Peplowski, P. N., D. J. Lawrence, L. G. Evans, R. L. Klima, D. T. Blewett, J. O. Goldsten, S. L. Murchie, T. J. McCoy, L. R. Nittler, and S. C. Solomon (2015), Constraints on the abundance of carbon in near-surface materials on Mercury: Results from the MESSENGER Gamma-Ray Spectrometer, *Planet. Space Sci.*, *108*, 98–107.
Peplowski, P. N., R. L. Klima, D. J. Lawrence, C. M. Ernst, B. W. Denevi, E. A. Frank, J. O. Goldsten, S. L. Murchie, L. R. Nittler, and S. C. Solomon (2016), Remote sensing evidence for an ancient carbon-bearing crust on Mercury, *Nat. Geosci.*, *9*(4), 273–276.
Ramirez, R. M., R. Kopparapu, M. E. Zugger, T. D. Robinson, R. Freedman, and J. F. Kasting (2014), Warming early Mars with CO_2 and H_2, *Nat. Geosci.*, *7*, 59–63.
Righter, K., K. Pando, and L. Danielson (2009), Experimental evidence for sulfur-rich Martian magmas: Implications for volcanism and surficial sulfur sources, *Earth Planet. Sci. Lett.*, *288*, 235–243.

Rosenthal, A., E. Hauri, and M. Hirschmann (2015), Experimental determination of C, F, and H partitioning between mantle minerals and carbonated basalt, CO_2/Ba and CO_2/Nb systematics of partial melting, and the CO_2 contents of basaltic source regions, *Earth Planet. Sci. Lett.*, *412*, 77–87.

Rothery, D. A., R. J. Thomas, and L. Kerber (2014), Prolonged eruptive history of a compound volcano on Mercury: Volcanic and tectonic implications, *Earth Planet. Sci. Lett.*, *385*, 59–67.

Rutherford, M. J., and P. Papale (2009), Origin of basalt fire-fountain eruptions on Earth versus the Moon, *Geology*, *37*, 219–222.

Sagan, C., and G. Mullen (1972), Earth and Mars: Evolution of atmospheres and surface temperatures, *Science*, *177*, 52–56.

Shcheka, S. S., M. Wiedenbeck, D. J. Frost, and H. Keppler (2006), Carbon solubility in mantle minerals, *Earth Planet. Sci. Lett.*, *245*, 730–742.

Shearer, C. K., P. C. Hess, M. A. Wieczorek, M. E. Pritchard, E. M. Parmentier, L. E. Borg, J. Longhi, L. T. Elkins-Tanton, C. R. Neal, and I. Antonenko (2006), Thermal and magmatic evolution of the Moon, *Rev. Mineral. Geochem.*, *60*, 365–518.

Sifré, D., E. Gardés, M. Massuyeau, L. Hashim, S. Hier-Majumder, and F. Gaillard (2014), Electrical conductivity during incipient melting in the oceanic low-velocity zone, *Nature*, *509*, 81–85.

Sleep, N. H., and K. Zahnle (2001), Carbon dioxide cycling and implications for climate on ancient Earth, *J. Geophys. Res.*, *106*, 1373–1399.

Squyres, S., J. Grotzinger, R. Arvidson, J. Bell, W. Calvin, P. Christensen, B. Clark, J. Crisp, W. Farrand, and K. E. Herkenhoff (2004), In situ evidence for an ancient aqueous environment at Meridiani Planum, Mars, *Science*, *306*, 1709–1714.

Stanley, B. D., M. M. Hirschmann, and A. C. Withers (2011), CO_2 solubility in Martian basalts and Martian atmospheric evolution, *Geochim. Cosmochim. Acta*, *75*, 5987–6003.

Stanley, B. D., D. R. Schaub, and M. M. Hirschmann (2012), CO_2 solubility in primitive Martian basalts similar to Yamato 980459, the effect of composition on CO_2 solubility of basalts, and the evolution of the Martian atmosphere, *Am. Mineral.*, *97*(11–12), 1841–1848.

Stanley, B. D., M. M. Hirschmann, and A. C. Withers (2014), Solubility of C–O–H volatiles in graphite-saturated Martian basalts, *Geochim. Cosmochim. Acta*, *129*, 54–76.

Thomas, R. J., D. A. Rothery, S. J. Conway, and M. Anand (2014), Long-lived explosive volcanism on Mercury, *Geophys. Res. Lett.*, *41*, 6084–6092, doi:10.1002/2014GL061224.

Thomas, R. J., D. A. Rothery, S. J. Conway, and M. Anand (2015), Explosive volcanism in complex impact craters on Mercury and the Moon: Influence of tectonic regime on depth of magmatic intrusion, *Earth Planet. Sci. Lett.*, *431*, 164–172.

Tsuno, K., and R. Dasgupta (2011), Melting phase relation of nominally anhydrous, carbonated pelitic-eclogite at 2.5–3.0 GPa and deep cycling of sedimentary carbon, *Contrib. Mineral. Petrol.*, *161*, 743–763.

Tsuno, K., and R. Dasgupta (2015), Fe–Ni–Cu–C–S phase relations at high pressures and temperatures—The role of sulfur in carbon storage and diamond stability at mid- to deep-upper mantle, *Earth Planet. Sci. Lett.*, *412*, 132–142, doi:10.1016/j.epsl.2014.12.018.

Vander Kaaden, K. E., and F. M. McCubbin (2015), Exotic crust formation on Mercury: Consequences of a shallow, FeO-poor mantle, *J. Geophys. Res. Planets.*, *120*, 195–209, doi:10.1002/2014JE004733.

Vander Kaaden, K. E., and F. M. McCubbin (2016), The origin of boninites on Mercury: An experimental study of the northern volcanic plains lavas, *Geochim. Cosmochim. Acta*, *173*, 246–263.

Wadhwa, M. (2008), Redox conditions on small bodies, the Moon and Mars, *Rev. Mineral. Geochem.*, *68*, 493–510.

Walker, D. W., R. Dasgupta, J. Li, and A. S. Buono (2013), Nonstoichiometry and growth of some Fe carbides. *Contrib. Mineral. Petrol.*, *166*, 935–957.

Weider, S. Z., L. R. Nittler, S. L. Murchie, P. N. Peplowski, T. J. McCoy, L. Kerber, C. Klimczak, C. M. Ernst, T. A. Goudge, and R. D. Starr (2016), Evidence from MESSENGER for sulfur-and carbon-driven explosive volcanism on Mercury, *Geophys. Res. Lett.*, *43*, 3653–3661, doi:10.1002/2016GL068325.

Wyllie, P. J., and W. L. Huang (1975), Influence of mantle CO_2 in the generation of carbonatites and kimberlites, *Nature*, *257*, 297–299.

Wetzel, D. T., M. J. Rutherford, S. D. Jacobsen, E. H. Hauri, and A. E. Saal (2013), Degassing of reduced carbon from planetary basalts, *Proc. Natl. Acad. Sci. U.S.A.*, *110*, 8010–8013.

Wetzel, D. T., E. H. Hauri, A. E. Saal, and M. J. Rutherford (2015), Carbon content and degassing history of the lunar volcanic glasses, *Nat. Geosci.*, *8*, 755–758.

Wood, B. J., J. Li, and A. Shahar (2013), Carbon in the core: Its influence on the properties of core and mantle, *Rev. Mineral. Geochem.*, *75*, 231–250.

Yoshioka, T., C. McCammon, S. Shcheka, and H. Keppler (2015), Letter. The speciation of carbon monoxide in silicate melts and glasses, *Am. Mineral.*, *100*, 1641–1644.

Zolotov, M. Y. (2011), On the chemistry of mantle and magmatic volatiles on Mercury, *Icarus*, *212*, 24–41.

Zolotov, M. Y., A. L. Sprague, S. A. Hauck, L. R. Nittler, S. C. Solomon, and S. Z. Weider (2013), The redox state, FeO content, and origin of sulfur-rich magmas on Mercury, *J. Geophys. Res. Planets.*, *118*, 138–146, doi:10.1029/2012JE004274.

Zurbuchen, T. H., J. M. Raines, G. Gloeckler, S. M. Krimigis, J. A. Slavin, P. L. Koehn, R. M. Killen, A. L. Sprague, R. L. McNutt, and S. C. Solomon (2008), MESSENGER observations of the composition of Mercury's ionized exosphere and plasma environment, *Science*, *321*, 90–92.